

REVIEWS OF TOPICAL PROBLEMS

PACS numbers: **46.25. – y, 46.35. + z,** 62.20.D – , 62.20.de

Anisotropy of elasticity of strongly nonstoichiometric disordered cubic carbides MC_y (M = Ti, Zr, Hf, Nb, Ta) and monoxides MO_y (M = Ti, V, Nb)

S.I. Sadovnikov, A.I. Gusev

DOI: https://doi.org/10.3367/UFNe.2025.08.039994

Contents

Abstract. **In recent years, significant progress has been achieved in the study of the anisotropy of elastic properties of nonstoichiometric cubic carbides MC_y (M = Ti, Zr, Hf, Nb, Ta) and monoxides MO_y (M = Ti, V, Nb). The composition of nonstoichiometric cubic compounds MX_y (X = C, O) determines their electronic structure, mechanical (elastic) properties and possible fields of application in modern engineering. This critical review summarizes recent achievements in the semi-empirical evaluation of elastic characteristics of nonstoichiometric cubic compounds. The main results on the dependences of elastic constants c_{ij} on the composition of disordered nonstoichiometric cubic carbides MC_y (M = Ti, Zr, Hf, Nb, Ta) and monoxides MO_y (M = Ti, V, Nb) are systematized for the first time. The effect of nonstoichiometry on the elastic anisotropy of carbides and monoxides is considered. It is shown that the maxima and minima of the spatial three-dimensional distributions of elastic moduli of the discussed nonstoichiometric cubic compounds are observed in the equivalent directions [±100], [0 ±10], [00 ±1] or directions [±1 ±1 ±1], respectively. It is shown that among the considered nonstoichiometric compounds, cubic titanium monoxide TiO_y has the largest anisotropy of elastic properties, which is a plastic material in terms of the ratio of shear and bulk moduli. An empirical relationship between the elastic stiffness constants c_{ij} of nonstoichiometric cubic carbides MC_y and their melting temperature is proposed.**

Keywords: nonstoichiometry, nonmetal sublattice defectivity, elastic properties anisotropy, melting temperature

S.I. Sadovnikov *, **A.I. Gusev** **
Institute of Solid State Chemistry,
Ural Branch of the Russian Academy of Sciences,
ul. Pervomaiskaya 91, 620990 Ekaterinburg, Russian Federation
E-mail: * sadovnikov@ihim.uran.ru, ** gusev@ihim.uran.ru

Received 23 May 2025, revised 9 July 2025
Uspekhi Fizicheskikh Nauk **196** (2) 149 – 172 (2026)
Translated by V.L. Derbov

1. Introduction

Most solids have no regions of homogeneity or significant deviations in composition from stoichiometry. Intensive studies of transition metal carbides, nitrides, oxides, and sulfides conducted in the first half of the 20th century revealed the existence of nonstoichiometric phases with wide regions of homogeneity. A group of highly nonstoichiometric compounds characterized by the presence of very wide regions of homogeneity is known [1–4]. Highly nonstoichiometric compounds include, in particular, cubic and hexagonal carbides, nitrides, and oxides of transition metals of groups IV–VI. Disordered cubic carbides of titanium, zirconium, hafnium, niobium, and tantalum have particularly wide regions of homogeneity; all of their properties change noticeably in the regions of homogeneity while maintaining an unchanged cubic structure. Of particular interest are carbides, which possess the highest hardness and refractoriness of all solid-phase substances. Due to their combination of excellent mechanical and thermal properties (especially very high hardness, high thermal and corrosion resistance, and high thermal and electrical conductivity), carbides have enormous potential for technical applications.

The influence of nonstoichiometry on the elastic properties of nonstoichiometric compounds has not been discussed in the literature until recently. All properties of nonstoichiometric compounds, including MC_y carbides, depend on their composition. Therefore, to consider the influence of nonstoichiometry on the elastic properties of nonstoichiometric compounds MX_y (X = C, N, O), their characteristics must be represented as functions of the composition (relative content of nonmetallic interstitial atoms X) $y = X/M$. The numerous available experimental data, summarized in books [1–8] and reviews [9–12], clearly indicate the dependence of the mechanical and elastic properties of nonstoichiometric carbides MC_y with the $B1$ structure on the relative carbon

content y. Indeed, the deviation of the composition of disordered carbides from stoichiometry is accompanied by a change in the elastic moduli E, B and G, as well as in Poisson's ratio μ [1–7, 11]. Single crystals of cubic compounds, including carbides and oxides, exhibit anisotropy of elastic properties, since their elastic properties are identical only along the principal axes [100], [010], and [001], but differ depending on the direction [hkl] due to differences in atomic packing. For example, an ab initio calculation of the spatial distribution of Young's modulus E_{hkl} of stoichiometric titanium nitride $TiN_{1.0}$ and titanium carbide $TiC_{1.0}$ was performed in Ref. [13].

Three-dimensional spatial distributions of the Young's elasticity moduli E_{hkl} of stoichiometric carbides titanium $TiCi_{1.0}$, chromium $CrC_{1.0}$, niobium $NbC_{1.0}$, molybdenum $MoC_{1.0}$, and hafnium $HfC_{1.0}$ were calculated and plotted in Ref. [14]. In Ref. [15], by ab initio calculations using the density functional theory (DFT) method, together with cubic (spatial group $Fm3m$) equiatomic titanium monoxide TiO the anisotropy of the elastic properties of TiO_2, Ti_2O_3, Ti_3O and Ti_3O_5 oxides was investigated and the spatial distributions of Young's elasticity modulus E_{hkl} of these oxides were constructed depending on the direction [hkl]. Three-dimensional distributions of the Young's elasticity modulus E_{hkl} and the shear modulus G_{hkl} of stoichiometric zirconium carbides $ZrC_{1.0}$ and hafnium carbides $HfC_{1.0}$ for different temperatures from 600 to 2400 K were calculated using the DFT method and plotted in Ref. [16]. In Ref. [17], three-dimensional spatial distributions of the Young's moduli E_{hkl} and the shear moduli G_{hkl}, as well as the Poisson ratio, were calculated and plotted for stoichiometric niobium, tantalum, and titanium carbides.

According to elasticity theory [18–20], the matrix (C) of the elastic stiffness constants of cubic crystals includes three independent elastic constants c_{11}, c_{12}, c_{44} and has the form

$$(C) = \begin{pmatrix} c_{11} & c_{12} & c_{12} & 0 & 0 & 0 \\ c_{12} & c_{11} & c_{12} & 0 & 0 & 0 \\ c_{12} & c_{12} & c_{11} & 0 & 0 & 0 \\ 0 & 0 & 0 & c_{44} & 0 & 0 \\ 0 & 0 & 0 & 0 & c_{44} & 0 \\ 0 & 0 & 0 & 0 & 0 & c_{44} \end{pmatrix}. \quad (1a)$$

The inverse matrix (S) of the elastic compliance constants s_{ij} of cubic crystals has a similar form and includes three elastic compliance constants s_{11}, s_{12} and s_{44}:

$$(S) = \begin{pmatrix} s_{11} & s_{12} & s_{12} & 0 & 0 & 0 \\ s_{12} & s_{11} & s_{11} & 0 & 0 & 0 \\ s_{12} & s_{12} & s_{11} & 0 & 0 & 0 \\ 0 & 0 & 0 & s_{44} & 0 & 0 \\ 0 & 0 & 0 & 0 & s_{44} & 0 \\ 0 & 0 & 0 & 0 & 0 & s_{44} \end{pmatrix}. \quad (1b)$$

Thus, to determine the anisotropy of the elastic properties of nonstoichiometric cubic carbides MC_y, it is necessary to know how the elastic stiffness constants c_{11}, c_{12} and c_{44} or the elastic compliance constants s_{11}, s_{12} and s_{44} change depending on the relative carbon content y.

Theoretical calculations of elastic characteristics and elastic stiffness constants c_{ij} are available only for stoichiometric cubic single crystals of $MC_{1.00}$ carbides. Theoretical estimates of the elastic properties of stoichiometric cubic carbides, carried out in Refs [21–46] and other publications, were obtained, as a rule, in various versions of the density functional theory using the local density approximation

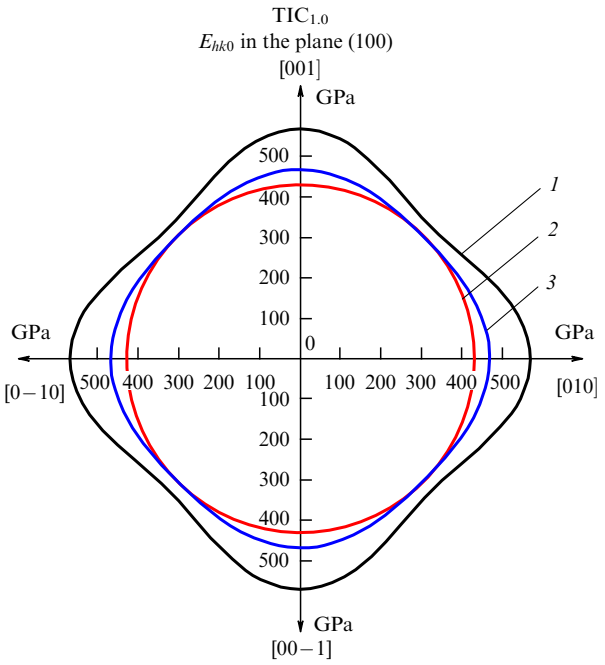

Figure 1. Difference in the distributions *1*, *2*, and *3* of Young's modulus E_{hkl} in the (100) plane of stoichiometric $TiC_{1.0}$ carbide, constructed based on the elastic stiffness constants c_{11}, c_{12}, and c_{44} presented in theoretical calculations [14, 17, 52], respectively.

(LDA) and the generalized gradient approximation (GGA) for exchange-correlation potentials at 0 K. Recently, the search for possible stable phases of nonstoichiometric compounds, including carbides, has also been carried out using an evolutionary algorithm implemented in the USPEX (Universal Structure Predictor: Evolutionary Xtallography) program [47]. The elastic properties of the predicted carbide phases are estimated by calculating the elasticity tensor coefficients using the finite difference method [48] implemented in the VASP (Vienna Ab initio Simulation Package) software package [49, 50]. However, these software products can only estimate the elastic properties of ordered carbide phases, while the elastic properties of disordered nonstoichiometric carbides remain unknown. In addition, the results of theoretical calculations of the elastic stiffness constants of the same stoichiometric carbide $MC_{1.0}$ differ significantly. For example, the elastic stiffness constants c_{ij} of stoichiometric titanium carbide $TiC_{1.0}$, calculated in 12 different theoretical studies, differ by 26–38% [51]. Figure 1 shows, as an example, the distributions of Young's modulus E_{hkl} in the (100) plane for stoichiometric carbide $TiC_{1.0}$, constructed based on the elastic stiffness constants c_{11}, c_{12}, c_{44} calculated theoretically [14, 17, 52] by the DFT method in the GGA approximation using experimental lattice parameters. It is evident that the results of the theoretical calculations differ substantially.

Resonance ultrasonic (US) spectroscopy can be used as an experimental method for studying the elasticity of carbides. In general, its use allows obtaining a complete set of elastic moduli nondestructively. Studies of carbides by US spectroscopy or resonance US spectroscopy make it possible to determine their mechanical properties, including elastic constants. Ultrasonic spectroscopy is based on the study of the propagation of ultrasonic waves through a material. In the case of carbides, ultrasonic waves can be

used to measure the time of their transit through the sample and to determine their propagation velocity, which is related to elastic properties of carbides such as Young's modulus, shear modulus, and Poisson's ratio. The advantage of using ultrasonic methods to study carbides is their nondestructive nature and the ability to apply over a wide temperature range. In general, ultrasonic spectroscopy and resonance ultrasonic spectroscopy are useful tools for studying the mechanical properties of carbides. However, the authors are unaware of any studies applying ultrasonic spectroscopy to nonstoichiometric disordered carbides. It is used in the study of composite materials such as SiC–AlN and TiC–TiNi.

Theoretical calculations of the elastic characteristics and elastic constants c_{ij} are available only for stoichiometric cubic carbides $MC_{1.00}$ and other ordered carbide phases at 0 K. The electronic structure of highly nonstoichiometric systems is very complex, and its calculation in different versions of DFT requires the introduction of many additional approximations and simplifications, leading to inaccurate final estimation of the elastic properties of the discussed highly nonstoichiometric carbide phases. In addition, the accuracy of the LDA and GGA approximations, widely used in DFT calculations, depends on the choice of the system being described and the choice of a suitable functional for a particular system. An insufficiently high cutoff energy can lead to inaccurate results. The use of pseudopotentials to model valence electrons can lead to errors in the calculation of electronic structure, especially for d- and f-elements.

Anisotropy of elastic properties is inherent not only in cubic carbides and oxides of transition metals. As an example, we can mention silver sulfide — argentite β-Ag_2S with a cubic structure (spatial group $Im3m$). The anisotropy of elasticity of this compound was previously studied in Refs [53, 54], where the velocities of longitudinal and transverse elastic vibrations were calculated, further used to find the elastic stiffness constants c_{11}, c_{12} and c_{44} and to construct the spatial distribution of the elastic modulus E_{hkl} of cubic silver sulfide β-Ag_2S at a temperature of 600 K (Fig. 2).

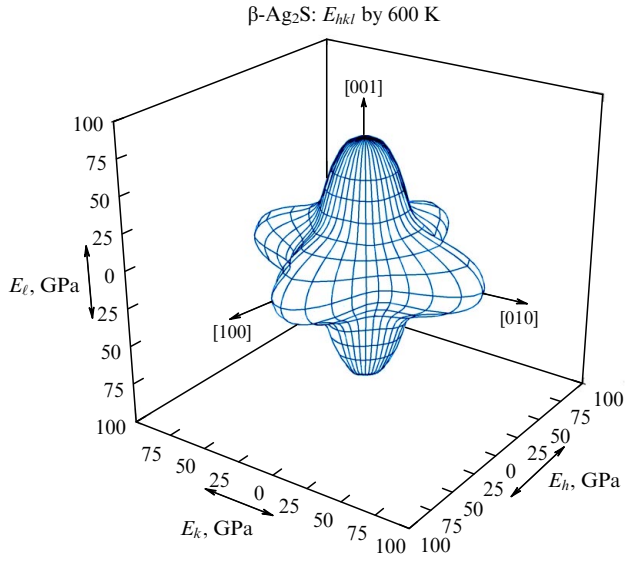

Figure 2. Spatial distribution of the elastic modulus E_{hkl} of cubic silver sulfide, argentite β-Ag_2S, at a temperature of 600 K [54].

2. Considering nonstoichiometry to estimate the elastic constants of cubic MX_y compounds

A semi-empirical method for estimating the elastic constants c_{ij} of disordered nonstoichiometric MC_y carbides with a cubic structure $B1$, depending on their composition, is proposed in Refs [51, 55–60]. The method uses a joint critical analysis of experimental results on the mechanical properties of carbides with different carbon contents and theoretical data on the elastic constants of stoichiometric $MC_{1.0}$ carbides. Briefly, the essence of this approach is as follows.

The first step is to determine the quantitative dependences of the elastic moduli of the MC_y carbide on the carbon content, which are found by approximating the corresponding experimental data for the carbide in question. These are the bulk modulus of elasticity B and the shear modulus G. The dependences of these moduli on the carbon content y in the MC_y carbide are as follows:

$$B(y) = B_{y=1}F_B(y)\,, \tag{2}$$

$$G(y) = G_{y=1}F_G(y)\,, \tag{3}$$

where $B_{y=1}$ and $G_{y=1}$ are the values of the bulk and shear moduli of the stoichiometric $MC_{1.0}$ carbide, obtained by approximation, and $F_B(y)$ and $F_G(y)$ are functions approximating the dependences of these moduli on the composition of the $MC_{1.0}$ carbide, taking into account the values of $B_{y=1}$ and $G_{y=1}$. The bulk and shear moduli of isotropic cubic crystals are related to the elastic stiffness constants as $B = (c_{11} + 2c_{12})/3$ and $G = c_{44}$ [27, 61, 62]. In Ref. [55], it was shown that the dependences of $B(y)$ and $G(y)$ of single-crystal MC_y carbides on the relative carbon content y have the same form as the quantitative dependences of $B(y)$ and $G(y)$ found by approximating the experimental data for these carbides. In other words, $(c_{11} + 2c_{12})/3 \sim B_{y=1}F_B(y)$ and $c_{44} \sim G_{y=1}F_G(y)$. According to Ref. [55], the dependences of the elastic constants $c_{11}(y)$ and $c_{12}(y)$ on the composition of cubic carbides are identical. As already noted, the results of theoretical calculations of the elastic stiffness constants of the same stoichiometric $MC_{1.0}$ carbide can differ significantly. Therefore, among the reported estimates of the theoretical values of the moduli of stoichiometric carbides $B_{\mathrm{calc},\,y=1}$, and $G_{\mathrm{calc},\,y=1}$, calculated in different versions of the density functional theory, we find those values of $B_{\mathrm{calc},\,y=1}$, and $G_{\mathrm{calc},\,y=1}$ that are closest to the approximate values of the moduli $B_{y=1}$ and $G_{y=1}$. These theoretical values of the moduli of stoichiometric carbides $B_{\mathrm{calc},\,y=1}$, and $G_{\mathrm{calc},\,y=1}$ correspond to the theoretical elastic stiffness constants $c_{ij}(y = 1)$, related empirically as $c_{11}(y = 1) \approx aB_{\mathrm{calc},\,y=1}$, $c_{12}(y = 1) \approx bB_{\mathrm{calc},\,y=1}$ and $c_{44}(y = 1) \approx cG_{\mathrm{calc},\,y=1}$. With these relations and relations (2) and (3) taken into account, the dependences of the elastic constants $c_{ij}(y = 1)$ on the composition of the MC_y carbide are represented as follows:

$$c_{11}(y) = c_{11}(y = 1)F_B(y)\,, \tag{4a}$$

$$c_{12}(y) = c_{12}(y = 1)F_B(y)\,, \tag{4b}$$

$$c_{44}(y) = c_{44}(y = 1)F_G(y)\,. \tag{4c}$$

Thus, using experimental data on the elastic properties of nonstoichiometric carbides MC_y, on the one hand, and

theoretical results on the elastic moduli and elastic stiffness constants $c_{ij}(y = 1)$ of stoichiometric $MC_{1.0}$ carbides, on the other hand, the dependences of the elastic stiffness constants $c_{ij}(y)$ were found. Particularly, in Refs [51, 55, 56, 58–60] the dependences of the elastic stiffness constants $c_{ij}(y)$ on the composition of the carbides of titanium TiC_y, niobium NbC_y, tantalum TaC_y, zirconium ZrC_y, and hafnium HfC_y were found. The elastic stiffness constants c_{11}, c_{12}, and c_{44} and the elastic compliance constants s_{11}, s_{12}, and s_{44} of cubic crystals are related to each other by the well-known relations [61]:

$$s_{11} = \frac{(c_{11} + c_{12})}{\left[(c_{11} - c_{12})(c_{11} + 2c_{12})\right]},$$
$$s_{12} = -\frac{c_{12}}{\left[(c_{11} - c_{12})(c_{11} + 2c_{12})\right]}, \quad s_{44} = \frac{1}{c_{44}}. \tag{5}$$

According to the elasticity theory [18–20, 61], cubic crystals have anisotropic elastic properties. Indeed, in the theory of elasticity, the specific energy of deformation of any crystals is represented through elastic components E_{ijkl} and constants S_{ijkl}, which have symmetric properties. In Ref. [62], it was shown that Young's modulus E_{hkl}, Poisson's ratio μ_{hkl}, and shear modulus G_{hkl} of cubic crystals depend on the crystallographic direction [hkl] and are therefore anisotropic. These elastic properties of cubic crystals, taking into account the anisotropy factor Γ, are determined through the elastic stiffness constants c_{11}, c_{12}, and c_{44} or the compliance tensor components s_{11}, s_{12}, and s_{44} as [62, 63]

$$E_{hkl} = \frac{(c_{11} - c_{12})(c_{11} + 2c_{12})c_{44}}{(c_{11} + c_{12})c_{44} - (2c_{44} - c_{11} + c_{12})(c_{11} + 2c_{12})\Gamma}$$
$$\equiv \frac{1}{s_{11} - 2(s_{11} - s_{12} - s_{44}/2)\Gamma}, \tag{6}$$

$$\mu_{hkl} = \frac{1}{2} - \frac{(c_{11} - c_{12})c_{44}}{2(c_{11}+c_{12})c_{44} - 2(2c_{44} - c_{11} + c_{12})(c_{11} + 2c_{12})\Gamma}$$
$$\equiv -\frac{s_{12} + (s_{11} - s_{12} - s_{44}/2)\Gamma}{s_{11} - 2(s_{11} - s_{12} - s_{44}/2)\Gamma}, \tag{7}$$

$$G_{hkl} = \frac{2(c_{11} - c_{12})c_{44}}{4c_{44} - 6(2c_{44} - c_{11} + c_{12})\Gamma}$$
$$\equiv \frac{1}{2s_{11} - 2s_{12} - 6(s_{11} - s_{12} - s_{44}/2)\Gamma}. \tag{8}$$

In Eqns (6)–(8), Γ is the anisotropy coefficient of cubic crystals, equal to $\Gamma = (h^2k^2 + h^2l^2 + k^2l^2)/(h^2 + k^2 + l^2)^2$ [62]. The bulk modulus B of cubic crystals is expressed as

$$B = \frac{c_{11} + 2c_{12}}{3} \equiv \frac{1}{3(s_{11} + 2s_{12})} \tag{9}$$

and does not depend on the direction [hkl], i.e., it is isotropic.

The anisotropy index Γ in cubic crystals for the [100] and [111] and equivalent directions is equal to 0 and 1/3. From Eqns (6) and (8) it follows that the specific values of E_{hkl} and G_{hkl} depend on the value of $(s_{11} - s_{12} - s_{44}/2)$. For cubic carbides MC_y with the $B1$ structure, the value of $(s_{11} - s_{12} - s_{44}/2)$ is negative, and for some body-centered (bcc) metals (e.g., tantalum), the value of $(s_{11} - s_{12} - s_{44}/2)$ is positive. With this fact and the anisotropy factor Γ taken into account, it follows from Eqns (6) and (8) that for substances with a negative or positive value of $(s_{11} - s_{12} - s_{44}/2)$, the appearance of the spatial distributions of Young's modulus E_{hkl} is different. As an example, Fig. 3 shows the model spatial distributions of Young's modulus E_{hkl} of cubic carbide TaC with the $B1$ structure and metallic body-centered cubic tantalum Ta. The appearance of these spatial distributions is different.

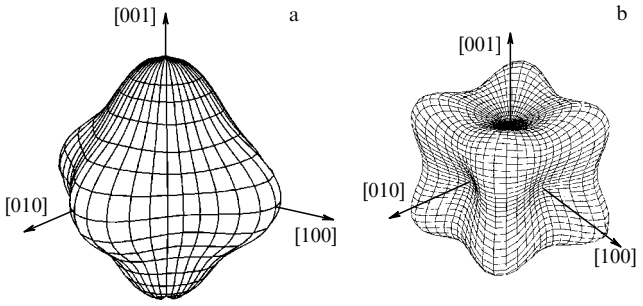

Figure 3. Model spatial distributions of the Young's modulus E_{hkl}: (a) cubic carbide TaC with the $B1$ structure, for which the value $(s_{11} - s_{12} - s_{44}/2) < 0$ in Eqn (6) is negative; (b) metallic body-centered cubic tantalum Ta with a positive value $(s_{11} - s_{12} - s_{44}/2) > 0$ in Eqn (6).

For nonstoichiometric cubic carbides and oxides MX_y with the $B1$ structure, the value of $(s_{11} - s_{12} - s_{44}/2) > 0$ is negative; therefore, for these compounds, the highest values of Young's moduli and shear moduli will be observed in the [100], [010], [001] and opposite directions, and the lowest values of these moduli are in the eight directions [$\pm1\ \pm1\ \pm1$]. For substances with $(s_{11} - s_{12} - s_{44}/2) > 0$, the highest Young's moduli are observed in the directions [$\pm1\ \pm1\ \pm1$], and the lowest moduli $E_{hkl}^{\min}$ are in the direction [100] and equivalent ones (see Fig. 2). Considering the anisotropy factor Γ for nonstoichiometric cubic compounds MX_y with the $B1$ structure, $E_{hkl}^{\max} = 1/s_{11}$ and $E_{hkl}^{\min} = 1/(s_{11} - (2/3) \times (s_{11} - s_{12} - (1/2)s_{44}))$, and the ratio of the largest and smallest Young's moduli is equal to $E_{hkl}^{\max}/E_{hkl}^{\min} = [s_{11} - (2/3)(s_{11} - s_{12} - (1/2)s_{44})]/s_{11} \equiv (1 - (2/3)(1 - s_{12}/s_{11} - (1/2)s_{44}/s_{11})$. Note that the ratio of the largest and smallest Young's moduli $E_{hkl}^{\max}/E_{hkl}^{\min}$ characterizes the magnitude of the anisotropy of the elastic properties: for isotropic cubic crystals $E_{hkl}^{\max}/E_{hkl}^{\min} = 1$, and the more the value of $E_{hkl}^{\max}/E_{hkl}^{\min}$ differs from unity, the greater the anisotropy of elasticity. The dependences of the elastic moduli on the crystallographic direction can also be represented through trigonometric functions of the direction angles [20]. The matrix (S_{tr}) of elastic compliance constants s_{ij} of the lowest-symmetry triclinic crystals has the general form

$$(S_{\text{tr}}) = \begin{pmatrix} s_{11} & s_{12} & s_{13} & s_{14} & s_{15} & s_{16} \\ s_{21} & s_{22} & s_{23} & s_{24} & s_{25} & s_{26} \\ s_{31} & s_{32} & s_{33} & s_{34} & s_{35} & s_{36} \\ s_{41} & s_{42} & s_{43} & s_{44} & s_{45} & s_{46} \\ s_{51} & s_{52} & s_{53} & s_{54} & s_{55} & s_{56} \\ s_{61} & s_{62} & s_{63} & s_{64} & s_{65} & s_{66} \end{pmatrix}. \tag{10}$$

In the monograph [20, p. 144], it is shown that the expression for the inverse Young's modulus of elasticity of crystals of the triclinic system, described by the matrix of elastic compliance constants (S_{tr}) (10), in the direction of the

unit vector l_i, has the form

$$\frac{1}{E} = s_{11}l_1^4 + 2s_{12}(l_1l_2)^2 + 2s_{13}(l_1l_3)^2 + 2s_{14}(l_1^2l_2l_3) + 2s_{15}(l_3l_1^3) + 2s_{16}(l_1^3l_2) + s_{22}l_2^4 + 2s_{23}(l_2l_3)^2 + 2s_{24}(l_2^3l_3) + 2s_{25}(l_1l_2^2l_3) + 2s_{26}(l_1l_2^3) + s_{33}l_2^4 + 2s_{34}(l_2l_3^3) + 2s_{35}(l_1l_3^3) + 2s_{36}(l_1l_2l_3^2) + s_{44}(l_2l_3)^2 + 2s_{45}(l_1l_2l_3^2) + 2s_{46}(l_1l_3l_2^2) + s_{55}(l_1l_3)^2 + 2s_{56}(l_2l_3l_1^2) + s_{66}(l_1l_2)^2\,, \quad (11)$$

where s_{ij} are the elastic compliance constants, and l_1, l_2 and l_3 are the direction cosines to the x, y, and z-axes, respectively. Formula (11) can be transformed into a similar formula for the inverse Young's modulus of elasticity of cubic crystals. Matrix (1b) of elastic compliance constants of cubic crystals includes only three constants s_{11}, s_{12}, s_{44} the rest are equal to 0. Replacing in Eqn (11) the triclinic constants $s_{14} = s_{15} = s_{16} = s_{24} = s_{25} = s_{26} = s_{34} = s_{35} = s_{36} = s_{45} = s_{46} = s_{56}$ by 0, and the triclinic constants $s_{11} = s_{22} = s_{33}$, $s_{12} = s_{13} = s_{23}$ and $s_{44} = s_{55} = s_{66}$ by the cubic constants s_{11}, s_{12} and s_{44}, respectively, we obtain an expression for the inverse Young's modulus of elasticity of cubic crystals:

$$\frac{1}{E_{hkl}} = s_{11} - 2\left(s_{11} - s_{12} - \frac{1}{2}\,s_{44}\right)(l_1^2l_2^2 + l_2^2l_3^2 + l_3^2l_1^2)\,. \quad (12)$$

Direction cosines l_1, l_2, and l_3, expressed through indices h, k, l of the crystallographic direction $[hkl]$, are equal to $l_1 = h/(h^2+k^2+l^2)^{1/2}$, $l_2 = k(h^2+k^2+l^2)^{1/2}$ and $l_3 = l/(h^2+k^2+l^2)^{1/2}$ [62]. The results of calculations considering Eqns (6) and (12) are the same. The same equations using direction cosines can be written for Poisson's ratio, shear moduli and compression moduli.

The concentration dependences $c_{ij}(y)$ (4) of MC_y carbides with different degrees of carbon sublattice defectivity found in Refs [51, 55, 58–60] were used for calculating by means of Eqns (6)–(9), the distributions of the elastic characteristics of single-crystal cubic MC_y carbides depending on the direction $[hkl]$ and the relative carbon content y.

3. Elastic anisotropy of nonstoichiometric carbides MC_y

Joint analysis of experimental data on the elastic properties of nonstoichiometric cubic titanium carbide TiC_y and theoretical calculations of the elastic constants c_{ij} of stoichiometric $TiC_{1.0}$ carbides [51] showed that the dependences of the elastic constants $c_{ij}(y)$ on the composition of nonstoichiometric cubic titanium carbide TiC_y can be written as

$$c_{11}(y) = c_{11}(y=1)[0.75938 + 0.40879y - 0.16817y^2]\,, \quad (13a)$$

$$c_{12}(y) = c_{12}(y=1)[0.75938 + 0.40879y - 0.16817y^2]\,, \quad (13b)$$

$$c_{44}(y) = c_{44}(y=1)[(-11.03975 + 25.74769y - 13.70794y^2) \times f_{\rm H}(y - y_{\rm b}) + (-0.82182 + 4.41716y - 2.76328y^2) \times f_{\rm H}(y_{\rm b} - y)]\,, \quad (13c)$$

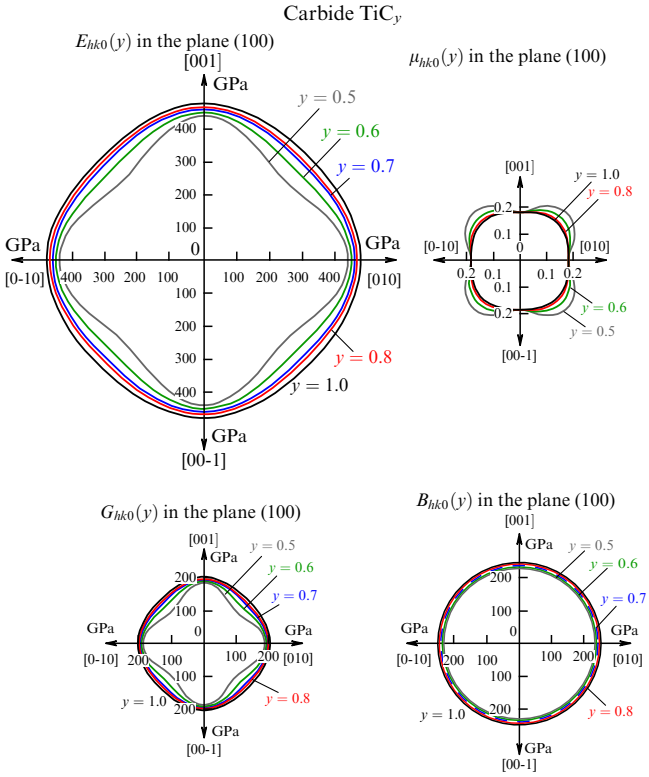

Figure 4. Dependences of Young's modulus E, Poisson's ratio μ, shear modulus G, and bulk modulus B on the crystallographic direction $[hkl]$ in the (100) plane of cubic carbide TiC_y with different relative carbon contents y from 0.5 to 1.0 [51].

where

$$f_{\rm H}(y - y_{\rm b}) = \begin{cases} 1, & \text{if } y \geqslant y_{\rm b}\,, \\ 0, & \text{if } y < y_{\rm b}\,, \end{cases}$$

$$f_{\rm H}(y_{\rm b} - y) = \begin{cases} 0, & \text{if } y > y_{\rm b}\,, \\ 1, & \text{if } y \leqslant y_{\rm b} \end{cases}$$

is the Heaviside function with $y_{\rm b} = 0.84$; $c_{11}(y=1) = 519$ GPa, $c_{12}(y=1) = 115$ GPa, and $c_{44}(y=1) = 183$ GPa.

The analysis of the dependences of c_{ij}, found for different cubic carbides and monoxides showed that the errors in determining the constants c_{11} are $\sim 12-15$ GPa, the errors in determining the constants c_{12} are smaller and are $\sim 8-0$ GPa, and the constants c_{44} have the smallest errors, equal to 3–5 GPa.

Based on the found dependences (13) of the elastic constants $c_{11}(y)$, $c_{12}(y)$, $c_{44}(y)$ of the carbide TiC_y with different nonstoichiometry of the carbon sublattice, in Ref. [49] the distributions of the elastic characteristics of the cubic carbide TiC_y were calculated and plotted, depending on the direction $[hkl]$ and the relative carbon content y.

Figure 4 shows the distributions of Young's modulus E, Poisson's ratio μ, shear modulus G, and bulk modulus B of cubic TiC_y carbide. The distributions are shown in the (100) plane for TiC_y carbides with $y = 0.5$, 0.6, 0.7, 0.8, and 1.0. Young's modulus E_{hk0} of $TiC_{1.0}$ carbide in the (100) plane varies from ~ 449.7 to 477.3 GPa, and Young's modulus of nonstoichiometric $TiC_{0.5}$ carbide with a defective carbon sublattice containing 50% vacancies in the same plane varies from ~ 345.7 to ~ 439.9 GPa. The maximum value of the

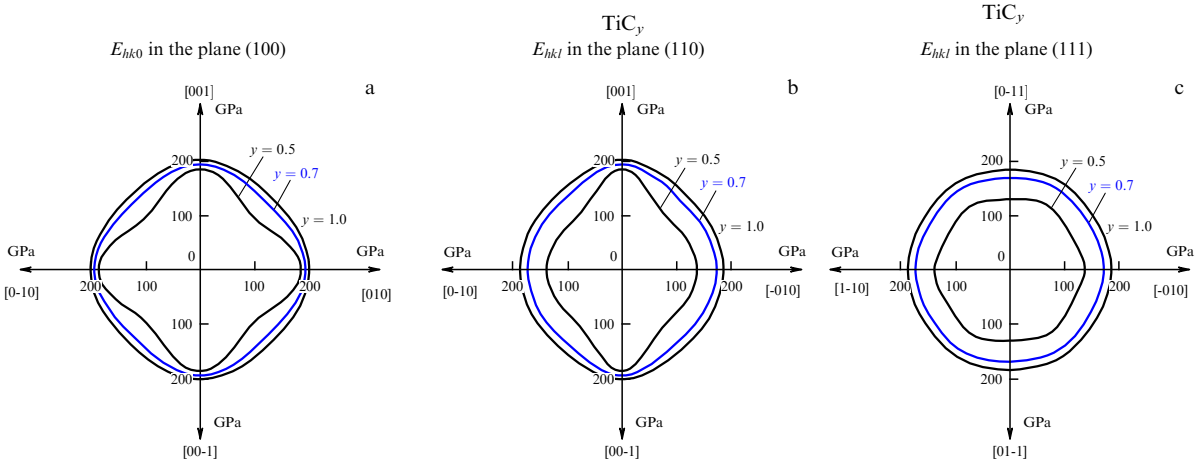

Figure 5. Distributions of the shear modulus G_{hkl} depending on the crystallographic direction [hkl] in the (a) (100), (b) (110), and (c) (111) planes of cubic TiC_y carbide with different carbon contents y [51].

shear modulus G_{hk0} increases slightly from $\sim$ 186.2 to $\sim$ 202.0 GPa upon going from nonstoichiometric $TiC_{0.5}$ carbide to stoichiometric $TiC_{1.0}$ carbide. The bulk modulus B of cubic TiC_y carbide is isotropic and depends only on the carbon content y. Figure 5 shows the dependences of the shear modulus G_{hkl} of TiC_y carbides with $y = 0.5$, 0.7, and 1.0 on the crystallographic direction [hkl] in the (100), (110), and (111) planes. The smallest value of G_{hkl} for TiC_y carbides is observed in the (111) plane. The shear modulus G_{hkl} in the (111) plane is virtually independent of direction and varies slightly from $\sim$ 184 to $\sim$ 187 GPa for $TiC_{1.0}$ and from $\sim$ 130 to $\sim$ 138 GPa for $TiC_{0.5}$ (Fig. 5c).

The three-dimensional spatial distributions of the Young's modulus E_{hkl} for stoichiometric $TiC_{1.0}$ carbide and nonstoichiometric $TiC_{0.50}$ carbide with a minimum carbon content y are shown in Fig. 6. The highest and lowest values of the Young's modulus of stoichiometric $TiC_{1.0}$ carbide are 477 and 450 GPa, respectively. As noted in Section 2, the highest modulus E^{max}_{hkl} is observed in the [001] and equivalent directions, and the lowest E^{min}_{hkl} value is observed in the directions [$\pm1 \pm 1 \pm 1$]. The small difference between E^{max}_{hkl} and E^{min}_{hkl} indicates that the stoichiometric titanium carbide is almost isotropic. Nonstoichiometric $TiC_{0.50}$ carbide with the largest and smallest Young's moduli $E^{max}_{hkl} = 440$ GPa and $E^{min}_{hkl} = 346$ GPa has a higher elastic anisotropy compared to stoichiometric $TiC_{1.0}$ carbide. Thus, the nonstoichiometry of TiC_y carbide is accompanied by an increase in the anisotropy of elastic properties.

Note that the influence of nonstoichiometry and ordering on the properties of highly nonstoichiometric compounds is quite comparable in magnitude. Chapter 11 of the monograph [2] examines in sufficient detail the influence of nonstoichiometry on all the properties of the discussed compounds in a disordered state. In particular, the influence of temperature on the hardness of nonstoichiometric compounds, especially carbides, has been repeatedly studied [64, 65], since the dependence $H_V(T)$ can be used to judge the mechanism of plastic deformation of the compound at a given temperature. With increasing temperature, the hardness of carbides rapidly decreases. The hardness of the transition metal carbides of group IV reaches the highest value for carbides $M^{(IV)}C_{1.0}$ of stoichiometric composition and decreases with decreasing carbon content y. The hardness of carbides NbC_y and TaC_y first increases with decreasing carbon content, reaches a maximum value of $\sim$ 33 GPa for $NbC_{0.77–0.79}$ and $\sim$ 29 GPa for $TaC_{0.81–0.84}$ and then decreases to 26–28 GPa at the lower boundary of the homogeneity region of the cubic phase. Vanadium carbide VC_y has a

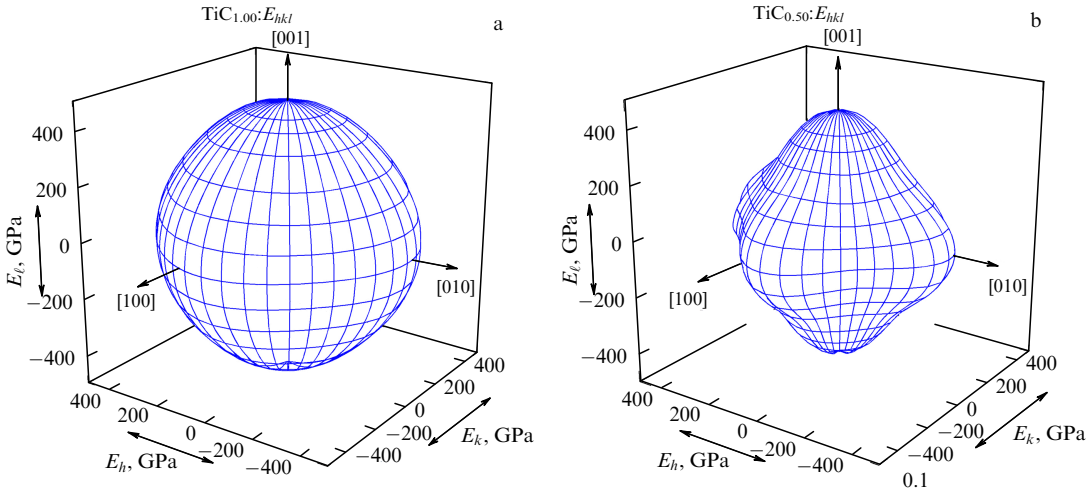

Figure 6. Spatial distribution of Young's modulus E_{hkl} of stoichiometric $TiC_{1.00}$ (a) and nonstoichiometric $TiCi_{0.50}$ (b) titanium carbides [51].

maximum hardness of 29–31 GPa at the upper boundary of the homogeneity region corresponding to carbide $VC_{0.875}$; with decreasing carbon content in VC_y the hardness decreases. An increase in the nonstoichiometry of titanium carbides TiC_y from $TiC_{1.00}$ to $TiC_{9.50}$ leads to an increase in the ratio $E_{hkl}^{\max}/E_{hkl}^{\min}$ from 1.06 to 1.27, i.e., to an increase in the anisotropy of the elastic properties of titanium carbide. On the contrary, in the case of zirconium carbide ZrC_y, an increase in nonstoichiometry from $ZrC_{1.00}$ to $ZrC_{0.60}$ leads to a decrease in the ratio $E_{hkl}^{\max}/E_{hkl}^{\min}$ from 1.08 to 1.05, i.e., is accompanied by a decrease in the elastic anisotropy of zirconium carbide. The difference in the behavior of titanium and zirconium carbides is due to the following. For titanium carbide, a nonlinear change in the shear modulus G was experimentally observed, for which a weak minimum in the shear modulus is observed near the $TiC_{0.83}$ composition. The shear modulus $G(y)$ dependence of zirconium carbide is smooth and does not have any extrema. The different concentration dependences of the shear moduli of titanium and zirconium carbides lead to different changes in the anisotropy of their elastic properties. Regarding disorder in sublattices, this work is devoted specifically to disordered nonstoichiometric cubic compounds, as follows from its title.

According to Ref. [59], the elastic constants $c_{11}(y)$, $c_{12}(y)$ and $c_{44}(y)$ as functions of the composition of disordered cubic zirconium carbide ZrC_y are expressed as

$$c_{11}(y) = c_{11}(y=1)(0.258337 + 1.501112y - 0.759449y^2), \quad (14a)$$

$$c_{12}(y) = c_{12}(y=1)(0.258337 + 1.501112y - 0.759449y^2), \quad (14b)$$

$$c_{44}(y) = c_{44}(y=1)(0.633395 + 0.678373y - 0.311768y^2), \quad (14c)$$

where $c_{11}(y=1) = 452$ GPa, $c_{12}(y=1) = 102$ GPa and $c_{44}(y=1) = 154$ GPa.

The elastic constants $c_{11}(y)$, $c_{12}(y)$ and $c_{44}(y)$ of ZrC_y carbide were used to calculate the distributions of the elastic characteristics of nonstoichiometric cubic zirconium carbide ZrC_y, depending on the direction $[hkl]$ and the carbon content y. Figure 7 shows the distribution of Young's moduli, shear moduli, and bulk compression moduli $E_{hk0}(y)$, $G_{hk0}(y)$ and $B_{hk0}(y)$ in the (100) plane of cubic zirconium carbides ZrC_y with y from 0.6 to 1.0. The Poisson's ratio $\mu_{hk0}(y)$ of ZrC_y carbide depends very weakly on y, so its distribution is shown only for $y = 0.6$ and 1.0 (see Fig. 7). The value of Young's modulus $E_{hk0}(y)$ of stoichiometric $ZrC_{1.0}$ carbide in the (100) plane varies from ~ 414 to ~ 383 GPa, and the value of Young's modulus E_{hk0} of $ZrC_{0.60}$ carbide with the greatest deviation from stoichiometry in the same plane varies from ~ 367 to ~ 350 GPa (see Fig. 7). The maximum value of the shear modulus G_{hk0} varies from 175 GPa for $ZrC_{1.00}$ carbide to 155 GPa for $ZrC_{0.60}$. The distributions of the moduli $E_{hk0}(y)$, $G_{hk0}(y)$, and $B_{hk0}(y)$ in the (100) plane of cubic ZrC_y are very similar to the analogous distributions for cubic titanium carbide TiC_y (see Fig. 4). Very small changes in E_{hk0}, μ_{hk0} and G_{hk0} depending on the direction $[hkl]$ indicate weak anisotropy of the elastic properties of cubic ZrC_y carbide. The elastic anisotropy of cubic ZrC_y carbide is even smaller than that of cubic titanium carbide TiC_y. The three-

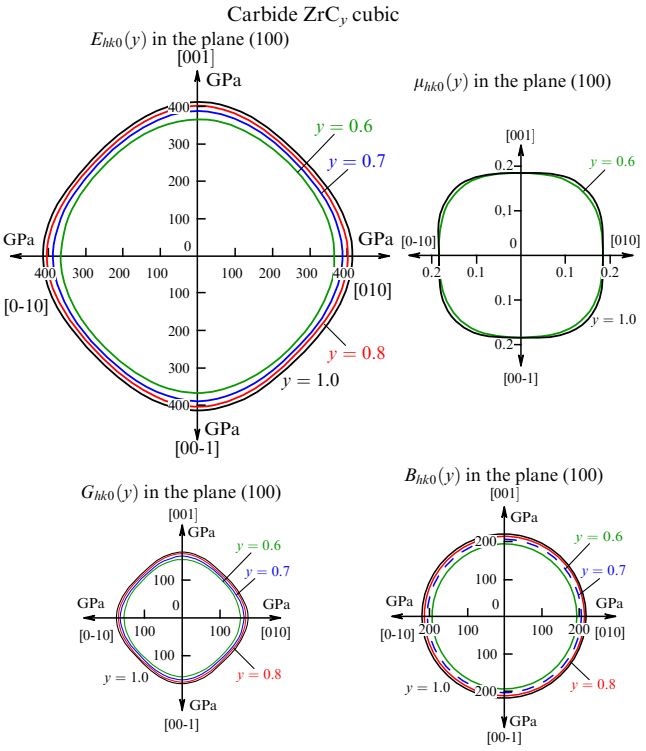

Figure 7. Dependences of Young's modulus E, Poisson's ratio μ, shear modulus G and bulk compression modulus B on the crystallographic direction $[hkl]$ in the (100) plane of cubic zirconium carbide ZrC_y, with different relative carbon contents y from 0.6 to 1.0 [59].

dimensional spatial distributions of Young's modulus E_{hkl} of stoichiometric $ZrC_{1.00}$ carbide and $ZrC_{0.60}$ carbide with the maximum deviation of composition from stoichiometry (Fig. 8) confirm weak anisotropy of elasticity of nonstoichiometric cubic zirconium carbide ZrC_y.

The experimental data on the mechanical and elastic properties of disordered nonstoichiometric cubic hafnium carbide $HfC_y$and the results of theoretical calculations of the elastic constants c_{ij} of stoichiometric carbides $HfC_{1.0}$ were analyzed in Ref. [60]. According to this analysis, the dependences of the elastic constants $c_{ij}(y)$ on the composition of nonstoichiometric cubic hafnium carbide HfC_y have the form

$$c_{11}(y) = c_{11}(y=1)(0.621824 + 0.378176y)\,, \quad (15a)$$

$$c_{12}(y) = c_{12}(y=1)(0.621824 + 0.378176y)\,, \quad (15b)$$

$$c_{44}(y) = c_{44}(y=1)(-1.046548 + 3.657427y - 1.610879y^2), \quad (15c)$$

where $c_{11}(y=1) = 485.6$ GPa, $c_{12}(y=1) = 106.4$ GPa, and $c_{44}(y=1) = 156.2$ GPa.

The concentration dependences $c_{ij}(y)$ (15) for disordered carbide HfC_y were used in Ref. [58] to calculate the distributions of the elastic characteristics of this carbide.

The plotted distributions of Young's modulus $E_{hk0}(y)$, shear modulus $G_{hk0}(y)$, and bulk modulus $B_{hk0}(y)$, as well as Poisson's ratio $\mu_{hk0}(y)$ in the (100) plane of cubic carbide HfC_y at $y = 0.6$, 0.7, 0.8 and 1.0 are shown in Fig. 9. The value of Young's modulus E_{hk0} of stoichiometric $HfC_{1.0}$ in the (100) plane varies from ~ 447 to ~ 397 GPa, and the value of

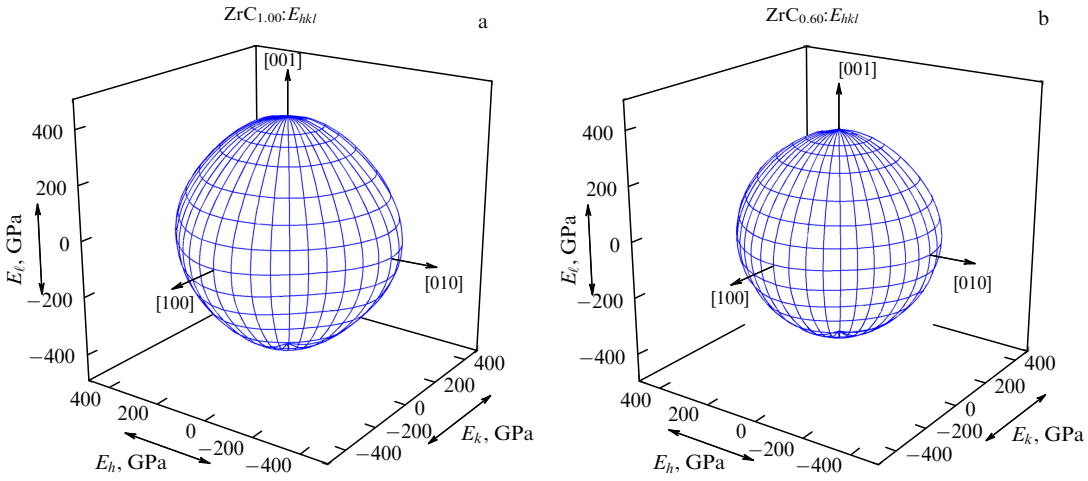

Figure 8. Three-dimensional spatial distribution of Young's modulus E_{hkl} (a) of stoichiometric $ZrC_{1.00}$ and (b) nonstoichiometric $ZrC_{0.60}$ zirconium carbides [59].

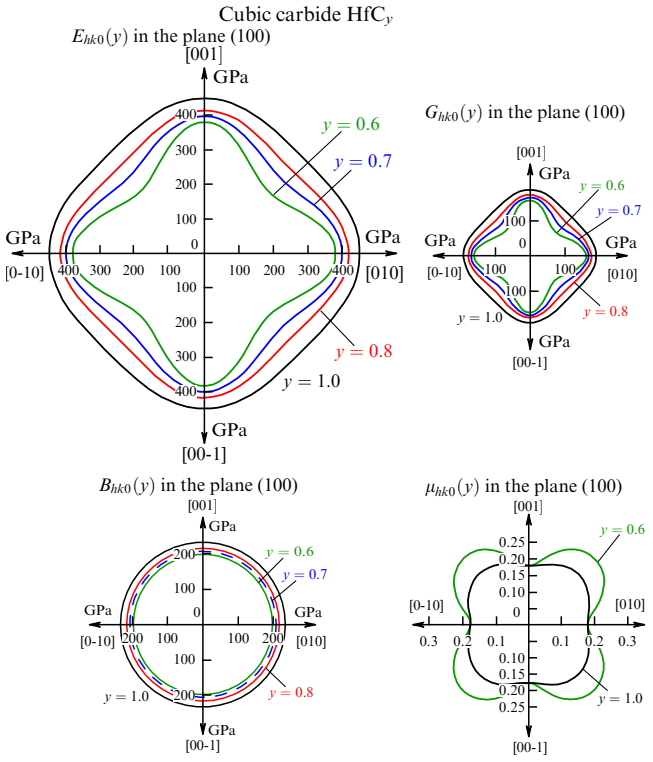

Figure 9. Young's, shear, and bulk moduli E, G, B and Poisson's ratio μ as functions of the crystallographic direction [hkl] in the (100) plane of cubic hafnium carbide HfC_y with relative carbon contents y varying from 0.6 to 1.0 [60].

Young's modulus E_{hk0} of the $HfC_{0.60}$ carbide with the maximum deviation from stoichiometry in the same plane varies from $\sim$ 380 to $\sim$ 256 GPa. The maximum value of the shear modulus G_{hk0} varies from 190 GPa for the $HfC_{1.0}$ carbide to 161 GPa for $HfC_{0.60}$. The values of bulk modulus B of the $HfC_{1.0}$ and $HfC_{0.60}$ carbides are $\sim$ 233 and $\sim$ 198 GPa, respectively. Poisson's ratio μ in the (100) plane of hafnium carbide varies from $\sim$ 0.180 to $\sim$ 0.284. Noticeable changes in E_{hk0}, μ_{hk0}, and G_{hk0} of nonstoichiometric $HfC_{0.60}$ carbide depending on the direction [hkl] indicate its significantly higher elastic anisotropy compared to the weakly anisotropic stoichiometric $HfC_{1.0}$. A significant change in elastic anisotropy in the homogeneity region of disordered cubic carbide HfC_y distinguishes it from titanium TiC_y and zirconium ZrC_y carbides [66].

The spatial three-dimensional distributions of Young's modulus E_{hkl} of $HfC_{0.60}$ and $HfC_{1.00}$ carbides corresponding to the lower and upper boundaries of the homogeneity region of HfC_y are shown in Fig. 10. It is evident that hafnium carbide HfC_y at the lower boundary of the homogeneity region exhibits significant elastic anisotropy, which decreases with increasing relative carbon content y. Thus, the value of Young's modulus E_{hkl} of HfC_y carbide increases, while the elastic anisotropy decreases with increasing carbon content y.

To assess quantitatively the anisotropy of the elastic properties of cubic crystals, they use the anisotropy criterion $A_{an} = 2c_{44}/(c_{11} - c_{12})$, proposed by Zener [67], the ratio $E^{max}_{hkl}/E^{min}_{hkl}$ of the largest and smallest Young's moduli, and the universal anisotropy criterion [68] $A^U = 5G_V/G_R + B_V/B_R - 6$, which is suitable for assessing the anisotropy of crystals with any symmetry (G_V, G_R, B_V, and B_R are the upper and lower limits of the shear and bulk moduli of a polycrystalline substance, calculated using the Voigt–Reuss–Hill averaging method [69]). Criterion $A = 1$ and ratio $E^{max}_{hkl}/E^{min}_{hkl} = 1$ correspond to completely isotropic cubic crystals, and the more the values of A_{an} and $E^{max}_{hkl}/E^{min}_{hkl}$ differ from 1, the greater the anisotropy of the elastic properties. The value of the universal criterion $A^U = 0$ indicates the isotropy of the crystal: the higher the value of A^U, the more intense the elastic anisotropy. The universal criterion of elastic anisotropy of cubic crystals A_{an} can be represented as $A^U = (6/5)[A_{an}^{1/2} - 1/A_{an}^{1/2}]^2$. Table 1 shows the changes in the anisotropy criteria A_{an} and A^U and the ratio $E^{max}_{hkl}/E^{min}_{hkl}$ for the homogeneity regions of cubic carbides TiC_y, ZrC_y, and HfC_y, according to the data of Refs [51, 59, 60]. It is seen that the greatest change in elastic anisotropy is observed for hafnium carbide HfC_y, and the smallest anisotropy and its smallest change correspond to cubic zirconium carbide ZrC_y.

In [55], an analysis of numerous experimental data on the mechanical and elastic properties of disordered nonstoichiometric cubic niobium carbide NbC_y, available in the literature, is presented, as well as the results of theoretical calculations of the elastic rigidity constants c_{ij} of stoichiometric carbides $NbC_{1.0}$. Based on these data, the authors of

Table 1. Changes in the elastic stiffness constants c_{ij} (GPa), anisotropy criteria A_{an} and A^{U}, and the ratios $E_{hkl}^{max}/E_{hkl}^{min}$ in the homogeneity regions of cubic carbides TiC_y, ZrC_y, HfC_y, NbC_y, and TaC_y according to [51, 55, 58–60].

Carbide MC_y	y	c_{11}	c_{12}	c_{44}	A_{an}	A^{U}	E_{hkl}^{max}	E_{hkl}^{min}	$E_{hkl}^{max}/E_{hkl}^{min}$
TiC_y [51]	0.5	478.4	106.0	127.4	0.684	0.175	439.9	322.6	1.36
	0.6	490.0	108.6	152.6	0.800	0.006	450.6	376.5	1.20
	0.7	499.9	110.8	167.7	0.862	0.027	459.7	408.1	1.13
	0.8	508.0	112.6	172.6	0.873	0.022	467.2	419.2	1.11
	1.0	519.0	115.0	183.0	0.906	0.012	477.3	441.2	1.08
ZrC_y [59]	0.6	400.3	90.3	142.9	0.922	0.008	367.0	344.1	1.07
	0.7	423.5	95.6	147.1	0.897	0.014	388.3	356.2	1.09
	0.8	439.9	99.3	150.4	0.833	0.019	403.3	365.2	1.10
	1.0	452.0	102.0	154.0	0.880	0.020	414.4	374.2	1.11
HfC_y [60]	0.6	412.1	90.3	88.7	0.551	0.438	379.7	231.5	1.64
	0.7	430.5	94.3	113.1	0.673	0.191	396.6	287.0	1.38
	0.8	448.9	98.4	132.5	0.756	0.094	413.5	329.7	1.25
	1.0	448.9	98.4	132.5	0.824	0.045	447.4	383.0	1.17
NbC_y [55]	0.7	351.5	87.9	121.3	0.920	0.008	316.4	295.9	1.07
	0.8	493.3	123.3	152.0	0.822	0.046	443.9	378.3	1.17
	1.0	598.0	149.5	178.2	0.795	0.064	538.2	446.0	1.21
TaC_y [58]	0.7	664.7	127.2	102.4	0.381	1.208	623.8	276.3	2.26
	0.8	708.9	135.6	149.5	0.522	0.527	665.4	389.2	1.71
	1.0	759.4	145.3	178.5	0.581	0.362	712.7	457.6	1.56

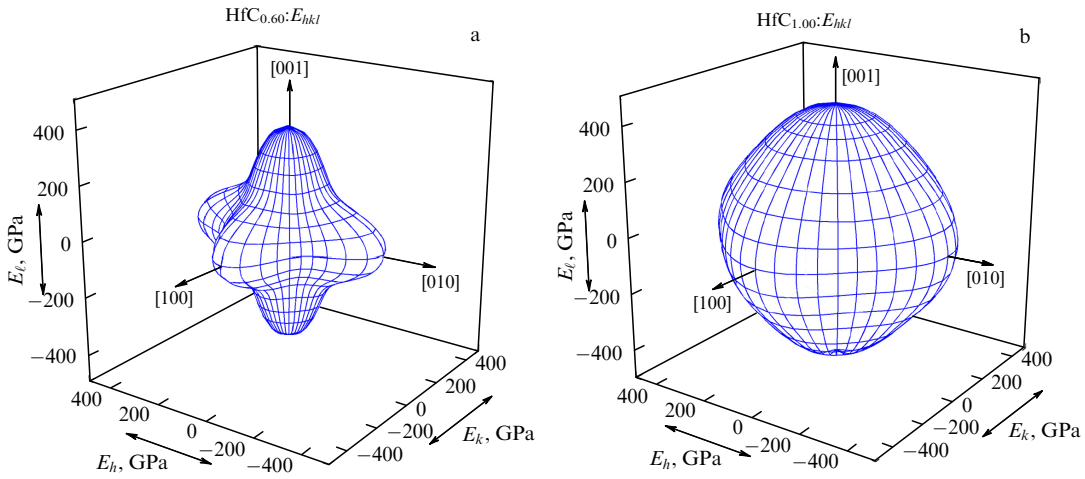

Figure 10. Spatial distributions of the Young's modulus E_{hkl} of (a) nonstoichiometric carbide $HfC_{0.60}$ and (b) stoichiometric carbide $HfC_{1.0}$ [60].

Ref. [55] found the dependences of the elastic constants $c_{ij}(y)$ on the composition of nonstoichiometric disordered cubic carbide NbC_y

$$c_{11}(y) = c_{11}(y=1)[1+0.1204(1-y)-4.981(1-y)^2], \quad (16a)$$

$$c_{12}(y) = c_{12}(y=1)[1+0.1204(1-y)-4.981(1-y)^2], \quad (16b)$$

$$c_{44}(y) = c_{44}(y=1)[1-0.0766(1-y)-3.292(1-y)^2], \quad (16c)$$

where $c_{11}(y=1) = 598$ GPa, $c_{12}(y=1) = 149.5$ GPa and $c_{44}(y=1) = 178.2$ GPa.

Figure 11 shows the distributions of the elastic Young's modulus $E_{hk0}(y)$ and the bulk modulus $B_{hk0}(y)$ in the (100) plane of cubic NbC_y carbide as y varies from 0.7 to 1.0. The distributions of the Young's modulus E in the (010) and (001) planes have the same shape. The value of the modulus E_{hk0} of stoichiometric $NbC_{1.0}$ in the (100) plane varies from $\sim$ 466 to $\sim$ 538 GPa, and for nonstoichiometric carbide $NbC_{0.70}$ the value of E_{hk0} varies from $\sim$ 301 to $\sim$ 316 GPa. It is evident from Fig. 11 that stoichiometric $NbC_{1.0}$ carbide has the greatest anisotropy of Young's modulus. The spatial distribution of the bulk modulus B of cubic niobium carbide has a spherical shape and does not depend on the direction $[hkl]$. The value of B_{hk0} varies from $\sim$ 176 GPa for $NbC_{0.70}$ to $\sim$ 299 GPa for stoichiometric $NbC_{1.0}$ carbide.

Figure 12 shows the shear modulus G_{hkl} and Poisson's coefficient μ_{hkl} of cubic niobium carbide NbC_y as functions of the crystallographic direction $[hkl]$. The distributions of the shear modulus G and Poisson's ratio μ are presented in the (100), (110), and (111) planes for NbC_y at $y = 0.7$ and 1.0. The shear modulus G of $NbC_{1.0}$ and $NbC_{0.7}$ carbides in the (100) plane varies from $\sim$ 224 to $\sim$ 178 GPa and from $\sim$ 132 to $\sim$ 111 GPa, respectively. The value of the shear modulus G_{hkl} in the (111) plane is practically independent of the direction and varies from $\sim$ 181 to $\sim$ 188 GPa for $NbC_{1.0}$ and from 134 to 135 GPa for $NbC_{0.7}$ (Fig. 12c). The Poisson's ratio μ_{hkl} of the $NbC_{1.0}$ and $NbC_{0.7}$ carbides varies in the

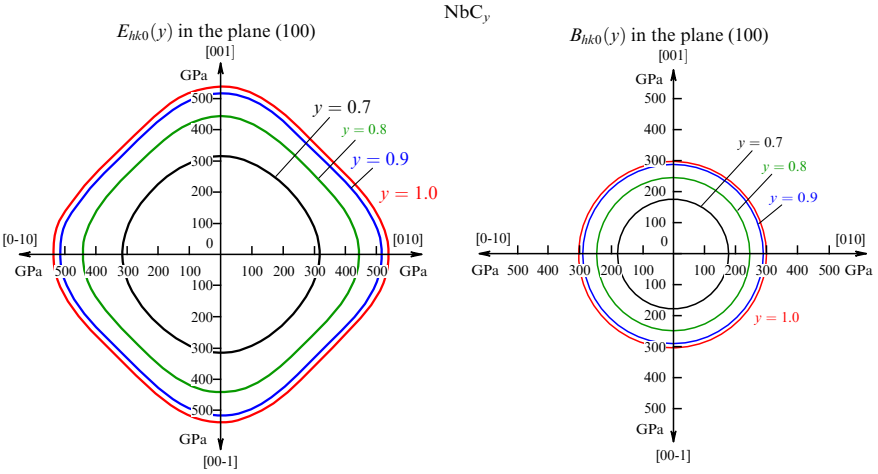

Figure 11. Young's moduli E and uniform compression moduli B as functions of the crystallographic direction [hkl] in the (100) plane of cubic niobium carbides NbC_y with different relative carbon contents y from 0.7 to 1.0 [55].

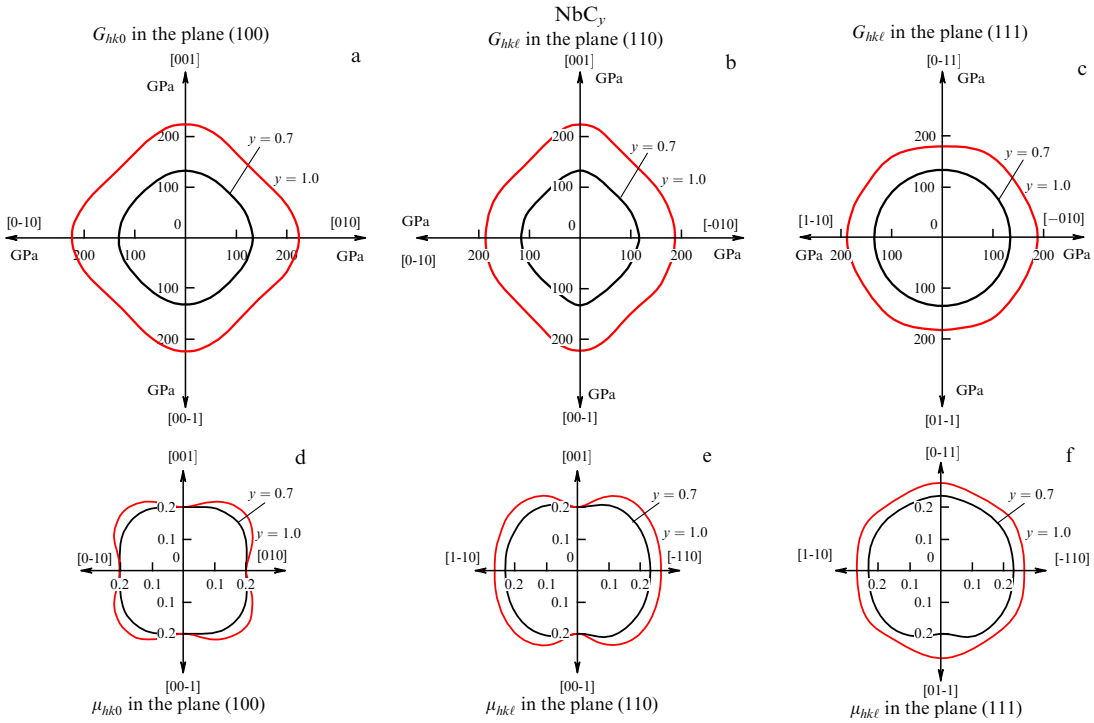

Figure 12. Changes in the shear modulus G and Poisson's ratio μ from the crystal direction [hkl] in the planes (a) (100), (b) (110), and (c) (111) of cubic niobium carbide NbC_y with y = 0.7 and 1.0 [55].

ranges of $\sim 0.200-0.280$ and $\sim 0.200-0.239$, respectively (Figs 12d–f).

Calculation of the spatial distributions of Young's modulus E_{hkl} showed that the modulus E_{hkl} of stoichiometric $NbC_{1.0}$ has a maximum value of $\sim$ 538 GPa in the [100] direction and equivalent directions, and the lowest value of $E_{hkl}^{\min} \sim$ 446 GPa in eight directions [$\pm1\,\pm1\,\pm1$]. Young's modulus of nonstoichiometric carbide $NbC_{0.70}$ has the highest and lowest values of $\sim$ 316 and $\sim$ 275 GPa in the same directions, respectively.

Figure 13 shows the spatial distributions of the shear modulus G_{hkl} of cubic niobium carbides $NbC_{1.0}$ and $NbC_{0.70}$. The shear modulus G_{hkl} of stoichiometric carbide $NbC_{1.0}$ has the highest value of $\sim$ 224 GPa in the [100] direction and equivalent directions. The shear modulus G_{hkl} has the lowest value of $\sim$ 154 GPa in the [111] and equivalent directions. The maximum and minimum values of the shear modulus G_{hkl} of nonstoichiometric carbide $NbC_{0.70}$ equal to $\sim$ 132 and $\sim$ 111GPa are observed in the same directions as for stoichiometric carbide $NbC_{1.0}$. It is evident that stoichiometric carbide $NbC_{1.0}$ has a higher elasticity anisotropy compared to nonstoichiometric carbide $NbC_{0.70}$.

In Ref. [58], experimental data on the elastic properties and anisotropy of deformation distortions of disordered nonstoichiometric cubic tantalum carbide TaC_y were analyzed, as well as the results of theoretical calculations of the elastic constants of stoichiometric carbide $TaC_{1.0}$. The dependences of the elastic constants $c_{ij}(y)$ on the composi-

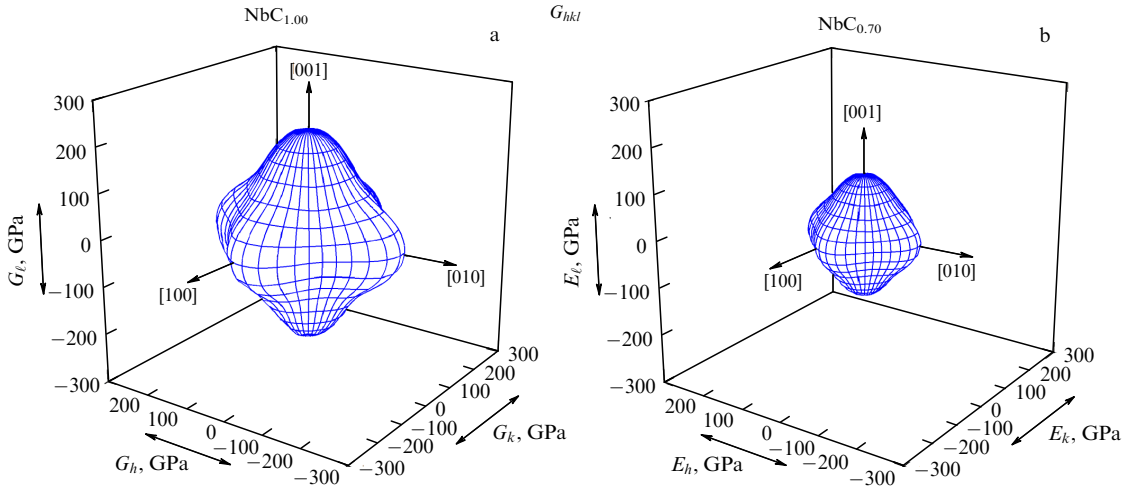

Figure 13. Spatial distribution of the shear modulus G_{hkl} of (a) stoichiometric carbide $NbC_{1.0}$ and (b) nonstoichiometric carbide $NbC_{0.70}$ [55].

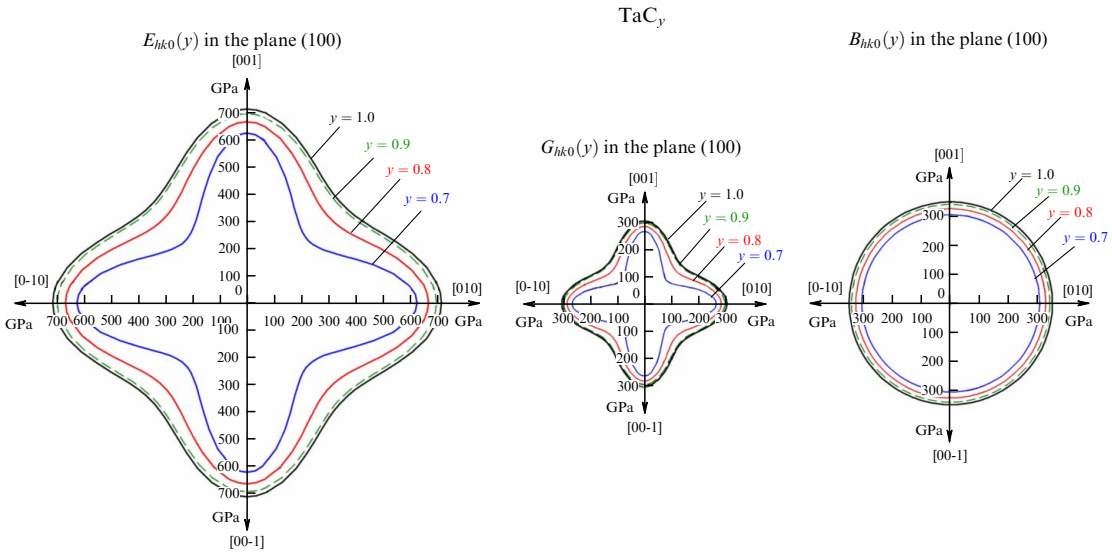

Figure 14. Dependences of Young's modulus E, shear modulus G, and bulk modulus B on the crystallographic direction $[hkl]$ in the plane (100) of the cubic TaC_y carbide with relative carbon content y varying from 0.7 to 1.0 [58].

tion of disordered carbide TaC_y were found:

$$c_{11}(y) = c_{11}(y=1)(1.89031y - 0.85992y^2)\,, \qquad (17a)$$

$$c_{12}(y) = c_{12}(y=1)(1.89031y - 0.85992y^2)\,, \qquad (17b)$$

$$c_{44}(y) = c_{44}(y=1)(-4.78732 + 12.03181y - 6.2246y^2), \qquad (17c)$$

where $c_{11}(y=1) = 737$ GPa, $c_{12}(y=1) = 141$ GPa and $c_{44}(y=1) = 175$ GPa.

Figure 14 shows the distributions of Young's modulus E, shear modulus G, and bulk modulus B of cubic carbide TaC_y. The distributions of E_{hk0}, G_{hk0}, and B_{hk0} moduli are shown in the (100) plane for TaC_y carbides with y varying from 0.7 to 1.0. Young's modulus E_{hk0} of $TaC_{1.0}$ carbide in the (100) plane varies from ~ 503 to ~ 713 GPa, and Young's modulus of nonstoichiometric carbide $TaC_{0.7}$ with a carbon sublattice containing 30% vacancies in the same plane varies from ~ 323 to ~ 624 GPa. The maximum value of the shear modulus E_{hk0} increases slightly from ~ 269 to ~ 307 GPa upon transition from nonstoichiometric $TaC_{0.7}$ carbide to stoichiometric $TaC_{1.0}$. It is clearly seen that an increase in the nonstoichiometry of tantalum carbide is accompanied by an increase in the anisotropy of the elastic properties. The bulk modulus B of cubic tantalum carbide TaC_y is isotropic: the value of B varies from ~ 306 GPa for $TaC_{0.7}$ to ~ 350 GPa for stoichiometric $TaC_{1.0}$.

The spatial distributions of Young's modulus E_{hkl} of stoichiometric tantalum carbide $TaC_{1.0}$ and nonstoichiometric carbide $TaC_{0.7}$ are shown in Fig. 15. The highest value of Young's modulus E_{max} of stoichiometric carbide $TaC_{1.0}$, equal to ~ 713 GPa, is observed in the [001] direction and equivalent directions, and the lowest Young's modulus E_{min}, equal to ~ 458 GPa, is observed in eight directions $[\pm 1 \pm 1 \pm 1]$. The maximum and minimum moduli E_{max} and E_{min} of nonstoichiometric carbide $TaC_{0.70}$ are ~ 624 and ~ 276 GPa, respectively, and are observed in the same directions as for stoichiometric carbide $TaC_{1.0}$. Non-stoichiometric carbide $TaC_{0.70}$ has a higher anisotropy of elastic properties than stoichiometric carbide $TaC_{1.0}$. The deviation of the tantalum carbide composition from close to the stoichiometry $TaC_{1.0-0.95}$ to the $TaC_{0.70}$ carbide with the

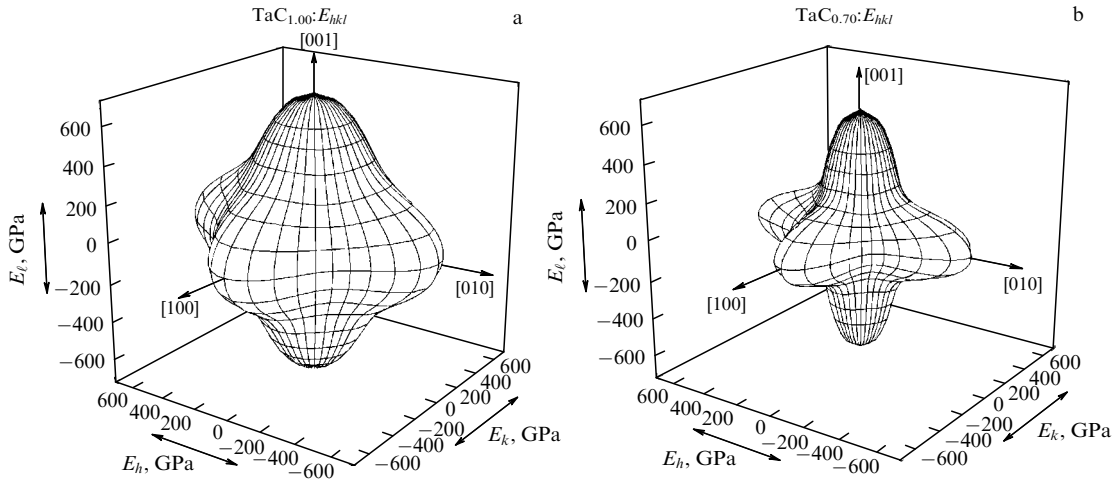

Figure 15. Spatial distribution of Young's modulus E_{hkl} of (a) stoichiometric carbide $TaC_{1.0}$ and (b) nonstoichiometric carbide $TaC_{0.70}$.

greatest defectiveness of the carbon sublattice is accompanied by a decrease in the anisotropy criterion A_{an} from ~ 0.58 to ~ 0.38. Thus, an increase in the anisotropy of the elastic properties of disordered tantalum carbide occurs with an increase in the defectiveness of its carbon sublattice.

4. Elastic anisotropy of cubic monoxides TiO_y, VO_y and Nb_3O_3

The approach to determining the elastic constants and estimating the elastic anisotropy of nonstoichiometric cubic carbides MC_y (M = Ti, Zr, Hf, Nb, Ta), implemented in Refs [51, 55, 56, 58–60], was applied to disordered nonstoichiometric cubic titanium monoxide TiO_y [70, 71].

Disordered cubic titanium monoxide TiO_y and titanium carbide TiC_y with a $B1$-type structure are related nonstoichiometric interstitial titanium compounds. The difference between them is due to the presence of structural vacancies (unoccupied atomic sites of the crystal lattice) in both the nonmetallic and metallic sublattices of titanium monoxide, whereas in titanium carbide vacancies are present only in the nonmetallic sublattice [1]. Due to the double defectiveness of TiO_y monoxide and the single defectiveness of TiC_y carbide, these compounds, all other things being equal, have different atomic packing densities, which should lead to differences in the anisotropy of their elastic properties.

Cubic (spatial group $Fm\bar{3}m$) titanium monoxide TiO_y with a $B1$-type structure has one of the widest homogeneity regions (from $TiO_{0.00}$ to $TiO_{1.25}$ at a temperature of ~ 1273 K) among nonstoichiometric cubic monoxides and monocarbides [1]. The composition of titanium monoxide, taking into account the presence of structural vacancies in each of the sublattices, has the form $Ti_xO_z \equiv TiO_y$ or $Ti_x\blacksquare_{1-x}O_z\square_{1-z} \equiv TiO_y$, where $y = z/x$, $\square$ and $\blacksquare$ are structural vacancies of the nonmetallic (oxygen) and metallic (titanium) sublattices, respectively. Titanium monoxide, formally having a stoichiometric equiatomic composition $TiO_{1.0}$, contains 16.7 at.% vacancies in sublattices of titanium and oxygen, therefore its real composition is $Ti_{0.833}O_{0.833}$.

In a disordered state, atoms and structural vacancies are distributed randomly over the sites of each of the sublattices of titanium monoxide Ti_xO_z. However, cubic symmetry is preserved, since the probability of finding an atom in all sites of its sublattice is the same and coincides with the relative content of occupied sites of the sublattice, i.e., it is equal to x for the titanium sublattice and equal to z for the oxygen sublattice. To estimate the elastic constants of TiO_y monoxide, the authors of Refs [70, 71] used experimental data [72] on the dependence of the microhardness of titanium monoxide on the relative oxygen content y and literature data on theoretically calculated elastic constants of stiffness c_{ij} and elastic moduli of equiatomic quasi-stoichiometric $TiO_{1.00}$ monoxide Based on a combined analysis of these data, the elastic constants $c_{ij}(y)$ were found as functions of the composition of disordered TiO_y monoxide:

$$c_{11}(y) = c_{11}(y=1)(-2.60339 + 6.11632y - 2.51292y^2)\,, \tag{18a}$$

$$c_{12}(y) = c_{12}(y=1)(-2.60339 + 6.11632y - 2.51292y^2)\,, \tag{18b}$$

$$c_{44}(y) = c_{44}(y=1)(-3.23902 + 7.17183y - 2.93282y^2)\,, \tag{18c}$$

where $c_{11}(y=1) = 511$, $c_{12}(y=1) = 53$ and $c_{44}(y=1) = 31$ GPa.

Expressions (18) were used to calculate the distributions of the elastic characteristics of single-crystal cubic TiO_y depending on the direction [hkl] and the relative oxygen content y. Figure 16 shows the distributions of Young's modulus $E_{hk0}(y)$, Poisson's ratio $\mu_{hk0}(y)$, shear modulus $G_{hk0}(y)$ and bulk modulus $B_{hk0}(y)$ in the (100) plane of cubic TiO_y monoxide with different relative oxygen content y. Due to the cubic symmetry of titanium monoxide, the distributions $E_{hk0}(y)$, $G_{hk0}(y)$, and $\mu_{hk0}(y)$ in the (010) and (001) planes are the same as in the (100) plane. The value of Young's modulus E_{hk0} of titanium monoxide $TiO_{0.80}$ corresponding to the lower boundary of the homogeneity region of the disordered cubic phase in the (100) plane varies from ~ 341 GPa to ~ 70 GPa. For equiatomic $TiO_{1.00}$ monoxide, the Young's modulus varies from ~ 499 to ~ 111 GPa, and for $TiO_{1.20}$ monoxide, from ~ 558 GPa to ~ 128 GPa (see Fig. 15). The maximum and minimum values of the shear modulus G_{hk0} vary from ~ 156 to ~ 25 GPa for $TiO_{0.80}$ monoxide, from ~ 229 to ~ 39 GPa for equiatomic $TiO_{1.00}$

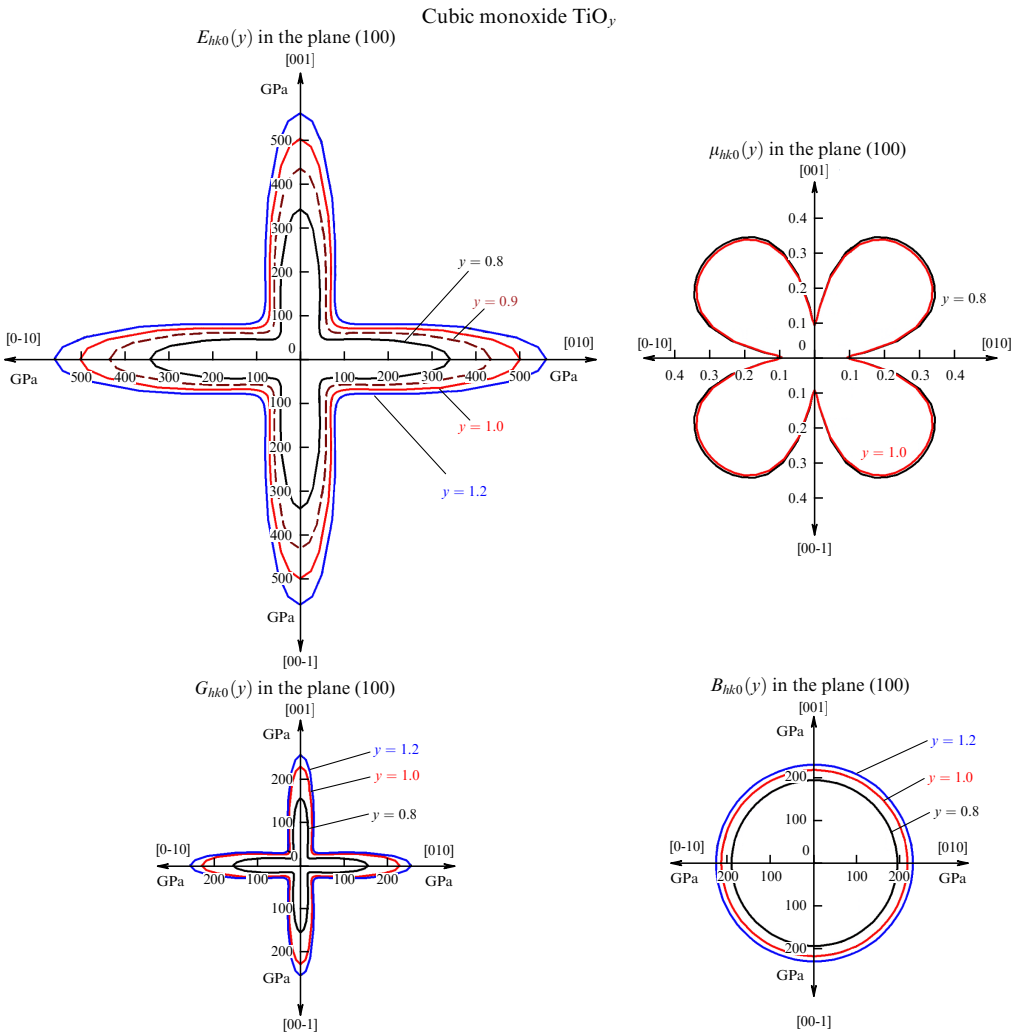

Figure 16. Young's modulus E ($y = 0.8$, 0.9, 1.0 and 1.2), Poisson's ratio μ ($y = 0.8$ and 1.0), shear modulus G ($y = 0.8$, 1.0, and 1.2) and bulk modulus B ($y = 0.8$, 1.0, and 1.2) as functions of the relative content y of oxygen in TiO$_y$ and crystallographic direction [hkl] in the plane (100) of the cubic titanium monoxide TiO$_y$ [70].

monoxide, and from ~ 256 to ~ 45 GPa for TiO$_{1.20}$ monoxide (see Fig. 16). The Poisson's ratio μ in the (100) plane of titanium monoxides varies in the range from ~ 0.094 to ~ 0.417 depending on the direction [hkl] and is practically independent of the TiO$_y$ composition. The bulk modulus B of cubic titanium monoxide is independent of the direction [hkl] and has a spherical shape; the B value of TiO$_{0.80}$, TiO$_{1.00}$, and TiO$_{1.20}$ monoxides is ~ 194, ~ 217, and ~ 230 GPa, respectively. Large changes in E_{hk0}, G_{hk0}, and μ_{hk0} depending on the direction [hkl] indicate strong anisotropy of the elastic properties of disordered cubic titanium monoxide TiO$_y$ at any relative oxygen content y in its homogeneity region.

The spatial three-dimensional distributions of the Young's modulus E_{hkl} and the bulk modulus B_{hkl} of disordered cubic titanium monoxides TiO$_{0.80}$, TiO$_{1.00}$, and TiO$_{1.20}$ are shown in Fig. 17. The TiO$_{0.80}$ monoxide corresponds to the lower boundary of the homogeneity region and has the lowest elastic stiffness constants c_{11}, c_{12}, and c_{44}, whereas the TiO$_{1.20}$ monoxide composition practically reaches the upper boundary of the homogeneity region and is distinguished by the highest values of the elastic stiffness constants c_{11}, c_{12}, and c_{44}. For all titanium monoxides, the highest Young's modulus $E_{\max}$ is observed along one of the crystallographic axes [00 ± 1], [0 ± 10] or [± 100]. The lowest value of $E_{\min}$ is observed in eight equivalent directions [$\pm 1 \pm 1 \pm 1$]. The highest and lowest Young's modulus values of the titanium monoxides TiO$_{0.80}$, TiO$_{1.00}$, and TiO$_{1.20}$ are ~ 341 and ~ 55, ~ 501 and ~ 88, ~ 560 and ~ 101 GPa, respectively (Fig. 17a). The values of the bulk moduli B_{hkl} of the monoxides TiO$_{0.80}$, TiO$_{1.00}$, and TiO$_{1.20}$ are ~ 194, ~ 217 and ~ 230 GPa, respectively. The anisotropy criterion A_{an} of disordered cubic titanium monoxides TiO$_y$ varies from 0.124 to 0.139 for monoxides ranging from TiO$_{0.80}$ to TiO$_{1.20}$. This indicates a very large anisotropy of the elastic properties of cubic titanium monoxide, which weakens somewhat with increasing relative oxygen content y in TiO$_y$.

The spatial distributions of Young's modulus E_{hkl} of cubic titanium monoxides can be compared with the spatial distributions of Young's modulus E_{hkl} of cubic titanium carbides TiC$_{0.50}$ and TiC$_{1.00}$ (see Fig. 6), corresponding to the lower and upper boundaries of the homogeneity region of TiC$_y$ carbide. According to Ref. [51], for nonstoichiometric TiC$_{0.50}$ carbide, the largest and smallest Young's moduli $E_{hkl}^{\max} = 440$ GPa and $E_{hkl}^{\min} = 346$ GPa, while for stoichiometric TiC$_{1.00}$ carbide, the largest and smallest moduli $E_{hkl}^{\max}$ and $E_{hkl}^{\min}$ are 477 and 450 GPa, respectively. Thus, $E_{hkl}^{\max}$ and $E_{hkl}^{\min}$ of titanium carbide TiC$_y$ differ very little from each other compared to the moduli of titanium monoxide TiO$_y$. It

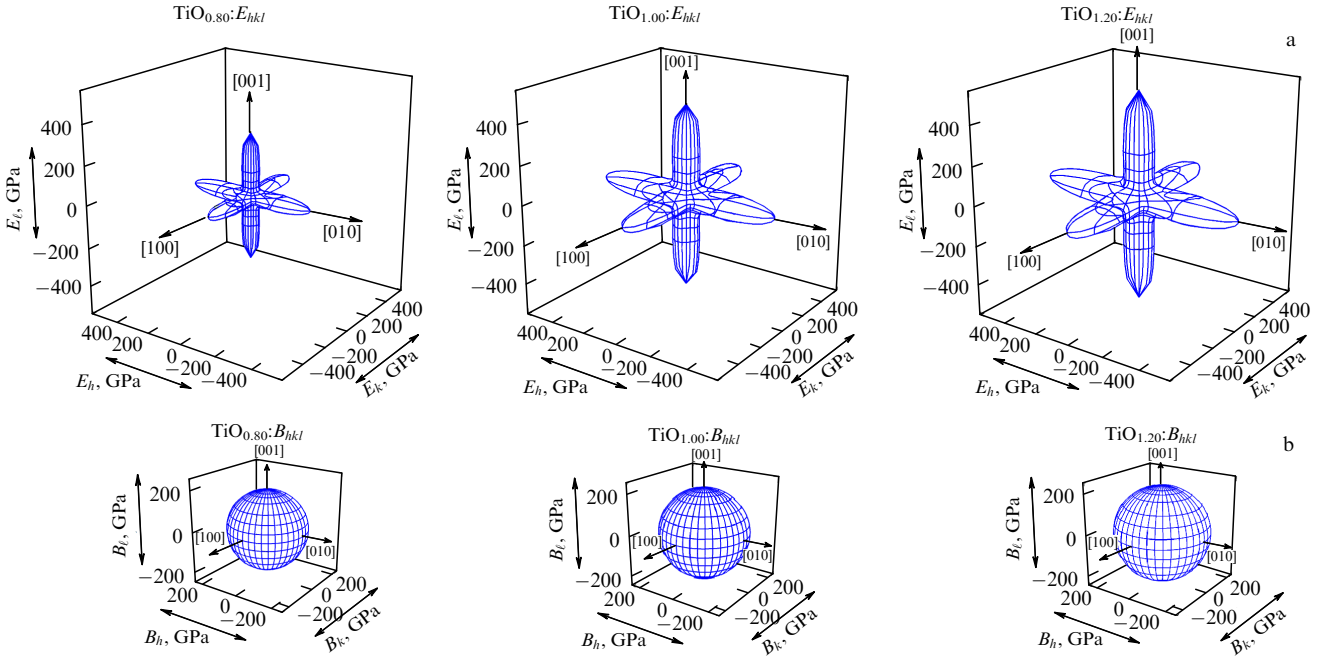

Figure 17. Spatial distributions of (a) Young's modulus E_{hkl} and (b) bulk modulus B_{hkl} for disordered cubic single crystals of titanium monoxides $TiO_{0.80}$, $TiO_{1.00}$ and $TiO_{1.20}$ [71].

is obvious that titanium monoxide TiO_y has a much greater anisotropy of elastic properties than its related cubic titanium carbide TiC_y.

In Ref. [73], it was shown that the ratio of the isotropic bulk modulus B to the isotropic shear modulus G can be used to predict the brittle and ductile behavior of polycrystalline materials. According to [71], high values of $B/G > 1.75$ correspond to ductile materials, while low values of $B/G < 1.75$ are inherent in brittle materials. Currently, the inverse ratio $k = G/B$ is also used as a criterion. The critical value of the inverse ratio G/B, which separates ductile substances from brittle ones, is approximately 0.57. Thus, substances with $k = G/B < 0.57$ are ductile. The isotropic elastic moduli B and G of polycrystalline titanium monoxide were calculated by the Voigt–Reuss–Hill method [70] using the found elastic stiffness constants c_{ij} (18). The B/G value of titanium monoxide TiO_y is high throughout the homogeneity region and varies from 2.70 to 2.58, and the inverse ratio $k = G/B$ varies from ~ 0.370 to ~ 0.387, so titanium monoxide can be considered a ductile material. This agrees with Ref. [15], in which the $k = G/B$ value of titanium monoxide $TiO_{1.00}$ is 0.382, and it is noted that $TiO_{1.00}$ monoxide is a malleable and ductile material.

The anisotropy of the elastic properties of cubic (spatial group $Fm3m$) vanadium monoxide with a wide homogeneity region was studied in Ref. [72]. Disordered cubic vanadium monoxide VO_y with the $B1$ structure, like titanium monoxide TiO_y, is a compound with double defectivity and has a wide homogeneity region $VO_{0.85}-VO_{1.23}$ [1].

Disordered vanadium monoxide is thermodynamically stable at $T > 1600$ K, and at temperatures below 1070 K, several ordered phases of different types with different symmetries are formed in different concentration and temperature ranges. Information on the mechanical properties of disordered cubic vanadium monoxide is limited to microhardness measurements of vanadium monoxide samples on quenched VO_y samples in the range $0.57 \leqslant y \leqslant 1.29$ [76] (Fig. 18). The data in Ref. [75] on the microhardness H_V

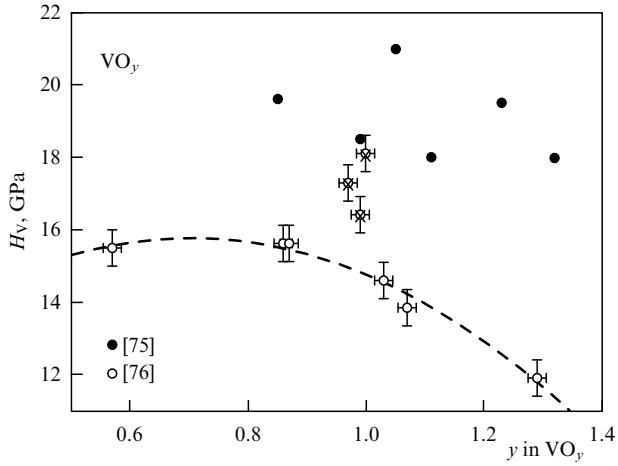

Figure 18. Microhardness $H_V(y)$ of disordered cubic vanadium monoxide VO_y, according to the data of Refs [75] and [76]. The data in Ref. [75] on the microhardness $H_V(y)$ are clearly overestimated, and the jump in $H_V(y)$ observed in the region of stoichiometric $VO_{\sim 1.00}$ in [76] is due to measurement errors. The dashed line approximates the microhardness $H_V(y)$ measured in [76].

are clearly overestimated, and the jump in H_V observed in [76] in the region of stoichiometric $VO_{\sim 1.00}$ is due to measurement errors. In general, as can be seen from Fig. 18, a nonlinear change in microhardness is observed with a change in y for VO_y.

Theoretical calculations of the elastic characteristics are presented in the only study [77] for the equiatomic quasi-stoichiometric monoxide $VO_{1.00}$ with the $B1$ structure. Theoretical estimates of the elastic properties in [77] were obtained within the framework of the density functional theory using the generalized gradient approximation (GGA) for exchange-correlation potentials and the VASP (Vienna *Ab initio* Simulation Package) code. According to [77], cubic vanadium monoxide VO has anisotropy of elastic properties. Its elastic constants c_{11}, c_{12}, and c_{44} are 484.6, 134.3, and 18.2 GPa, respectively.

According to Ref. [76], the dependence of the microhardness of disordered cubic vanadium monoxide VO_y can be approximated by the function

$$H_V(y) = 10.0500 + 16.2659y - 11.5620y^2 \ \ [\text{GPa}]. \quad (19)$$

The study of carbides, nitrides and other compounds [76] revealed a general tendency towards a decrease in their hardness H_V with a decrease in the shear modulus G and bulk modulus B. According to Refs [51, 78], for nonstoichiometric compounds the dependence of microhardness on the shear modulus has the form $H_V(y) = 0.151G(y)$. Using this function makes it possible to find the change in the shear modulus $G(y)$ depending on the composition of the disordered monoxide VO_y according to the data [76] on the change in its microhardness as

$$G(y) = \frac{H_V(y)}{0.151}. \quad (20)$$

Formula (20) was proposed in Ref. [78]. In Ref. [79], the relationship between the microhardness H_v and the shear modulus G was verified for carbides TiC, ZrC, NbC, TaC and many other compounds, including nonstoichiometric cubic nitrides and oxides.

According to the quantitative calculation [74] using function (20), the shear modulus $G_{y=1}$ of the stoichiometric monoxide $VO_{1.00}$ equals 97.1 GPa, and the dependence $G(y)$ of disordered vanadium monoxide VO_y on its composition y has the form

$$\begin{aligned} G(y) &= 66.55629 + 107.72119y - 76.56954y^2 \\ &= G_{y=1}(0.68544 + 1.10938y - 0.78856y^2) \ [\text{GPa}]. \end{aligned} \quad (21)$$

From the dependencies of microhardness $H_V(y)$ (19) and shear modulus $G(y)$ (20) of quenched disordered monoxide VO_y it is possible to find the bulk modulus $B(y)$ as a function of the relative oxygen content y. For this purpose, we can use the empirical function $H_V = [2(k^2G)^{0.585} - 3]$, where $k = G/B$, proposed in Ref. [79]. Transformation of this function allows us to establish the dependence of $B(y)$ on $G(y)$ and $H_V(y)$ in the form

$$B(y) = \frac{\left[G(y)\right]^{3/2}}{\left[(H_V(y) + 3)/2\right]^{1.17}}. \quad (22)$$

The dependence of the bulk modulus B of disordered vanadium monoxide VO_y, calculated using relation (22) from the concentration dependence $H_V(y)$ (19) of the microhardness of quenched vanadium monoxide [76] using the found quantitative dependence $G(y)$ (21), has the form

$$\begin{aligned} B(y) &= 58.5517 + 52.3784y - 35.8511y^2 \\ &= B_{y=1}(0.779868 + 0.697644y - 0.477512y^2) \ [\text{GPa}]. \end{aligned} \quad (23)$$

From (23) it follows that the bulk modulus $B_{y=1}$ of stoichiometric vanadium monoxide $VO_{1.00}$ is equal to 75.08 GPa. In the first approximation, the dependence $B(y)$ of single-crystal particles of vanadium monoxide VO_y on the relative oxygen content y has the same form as the dependence $B(y)$ (23), found on the basis of experimental data [76] on the microhardness of $H_V(y)$.

Taking into account the found elastic moduli $B_{\text{calc}, y=1} = 250.6$ GPa and $G_{\text{calc}, y=1} = 54.6$ GPa and the elastic constants $c_{11} = 484.6$, $c_{12} = 134.3$ and $c_{44} = 18.2$ GPa [77] of equiatomic stoichiometric vanadium monoxide, the theoretical elastic constants $c_{ij}(y = 1)$ and the theoretical values of the bulk modulus and shear modulus of stoichiometric $VO_{1.00}$, presented in Ref. [77], can be empirically related as $c_{11}(y = 1) = 1.93376B_{\text{calc}, y=1}$, $c_{12}(y = 1) = 0.53591B_{\text{calc}, y=1}$ and $c_{44}(y = 1) = 0.333333G_{\text{calc}, y=1}$. Earlier, using the example of disordered cubic titanium monoxide TiO_y and carbide TiC_y, it was shown that the dependences of the elastic constants c_{11} and c_{12} on the composition of the nonstoichiometric compound are qualitatively the same, therefore the constants $c_{11}(y)$ and $c_{12}(y)$ as functions of the composition of the disordered monoxide VO_y are equal to

$$c_{11}(y) = c_{11}(y = 1)(0.779868 + 0.697644y - 0.477512y^2), \quad (24a)$$

$$c_{12}(y) = c_{12}(y = 1)(0.779868 + 0.697644y - 0.477512y^2), \quad (24b)$$

$$c_{44}(y) = c_{44}(y = 1)(0.68544 + 1.10938y - 0.78856y^2), \quad (24c)$$

where $c_{11}(y = 1) = 484.6$ GPa, $c_{12}(y = 1) = 134.3$ GPa and $c_{44}(y = 1) = 18.2$ GPa.

The dependences of Young's modulus E_{hkl}, Poisson's ratio μ_{hkl}, and shear modulus G_{hkl} of cubic vanadium monoxide on the direction [*hkl*] were calculated using relations (6)–(8).

Figure 19 shows the constructed distributions of Young's modulus $E_{hkl}(y)$ and shear modulus $G_{hkl}(y)$ in the (100) plane of cubic vanadium monoxide VO_y with different oxygen contents y. Poisson's ratio $\mu_{hkl}(y)$ of vanadium monoxide is almost independent of the composition y, therefore its distribution is shown only for $y = 1.0$ (see Fig. 19). Due to the cubic symmetry, the distributions of the elastic characteristics $E_{hkl}(y)$, $G_{hkl}(y)$, and $\mu_{hkl}(y)$ of vanadium monoxide in the (010) and (001) planes are the same as in the (100) plane.

The Young's modulus E_{hk0} of vanadium monoxide $VO_{0.80}$, located near the lower boundary of the homogeneity region of the disordered cubic phase, in the (100) plane varies from ~ 440 to ~ 72 GPa. For equiatomic monoxide $VO_{1.00}$, the Young's modulus varies from ~ 426 to ~ 69 GPa, and for monoxide $VO_{1.20}$ from ~ 396 to ~ 60 GPa (see Fig. 19). The maximum and minimum values of the shear modulus G_{hk0} are from ~ 180 to ~ 25 GPa for $VO_{0.80}$ monoxide, from ~ 175 to ~ 24 GPa for equiatomic $VO_{1.00}$ and from ~ 163 to ~ 21 GPa for $VO_{1.20}$ (see Fig. 19). The Poisson's ratio μ in the (100) plane of vanadium monoxides, depending on the direction [*hkl*], varies in the range from ~ 0.177 to ~ 0.455 and is almost independent of the VO_y composition (see Fig. 19). The bulk modulus B of cubic vanadium monoxide has a spherical shape; the value of B for monoxides $VO_{0.80}$, $VO_{1.00}$, and $VO_{1.20}$ is ~ 259, ~ 251 and ~ 233 GPa, respectively. Very noticeable changes in E_{hk0}, G_{hk0}, and μ_{hk0} depending on the direction [*hkl*] indicate a strong anisotropy of the elastic properties of disordered cubic vanadium monoxide VO_y with any oxygen content y. Note that the constructed distributions of Young's modulus $E_{hkl}(y)$ and the shear modulus $G_{hkl}(y)$ in the (100) plane of cubic monoxide VO_y are very similar to respective distributions calculated earlier for cubic titanium monoxide TiO_y.

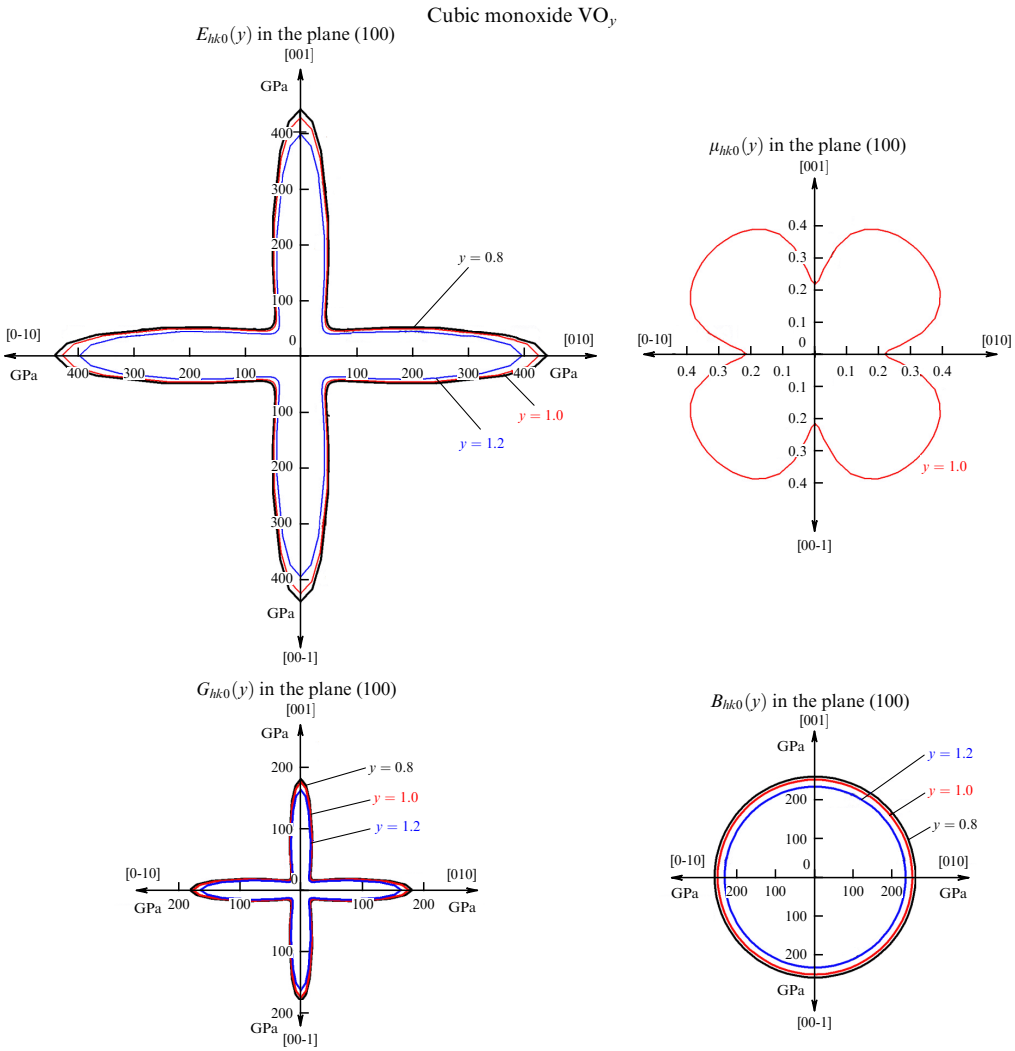

Figure 19. Dependences of Young's modulus E (y = 0.8, 1.0, and 1.2), the Poisson ratio μ (y = 1.0), shear modulus G (y = 0.8, 1.0, and 1.2) and bulk modulus B (y = 0.8, 1.0, and 1.2) on the crystallographic direction [hkl] in the plane (100) of the cubic vanadium monoxide VO$_y$ with different relative oxygen content y [74].

The spatial three-dimensional distribution of Young's modulus E_{hkl} of disordered cubic vanadium monoxide $VO_{1.00}$ is shown in Fig. 20. The highest Young's modulus E_{max} is observed along one of the crystallographic axes [00 ±1], [0 ±10], or [±100]. The lowest value of E_{min} is observed in eight equivalent directions [±1 ±1 ±1]. The highest and lowest values of Young's modulus of vanadium monoxide $VO_{1.00}$ are ~ 435 and ~ 82 GPa, respectively (see Fig. 20). In general, from the performed analysis of the change in elastic properties depending on the VO$_y$ composition, it follows that disordered cubic vanadium monoxide has a more pronounced anisotropy throughout the homogeneity region than titanium monoxide TiO$_y$.

In disordered cubic carbides TiC$_y$, ZrC$_y$, HfC$_y$, NbC$_y$, TaC$_y$ and in titanium monoxide TiO$_y$, the nonstoichiometry changes in the region of their homogeneity. In contrast, cubic niobium monoxide NbO with a high content of vacancies in each sublattice has virtually no homogeneity region. This unique compound contains the largest number of structural vacancies among all known compounds. According to Refs [80–83], the metallic and nonmetallic sublattices of cubic niobium monoxide contain 25% vacancies each.

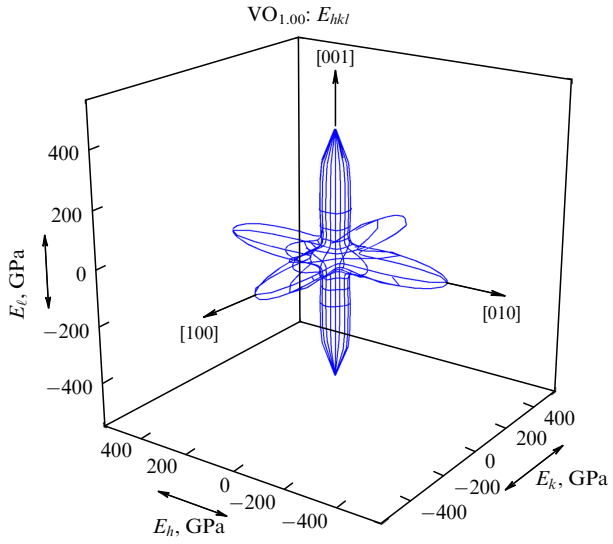

Figure 20. Spatial distribution of the Young's modulus E_{hkl} of the disordered cubic vanadium monoxide $VO_{1.00}$ [74].

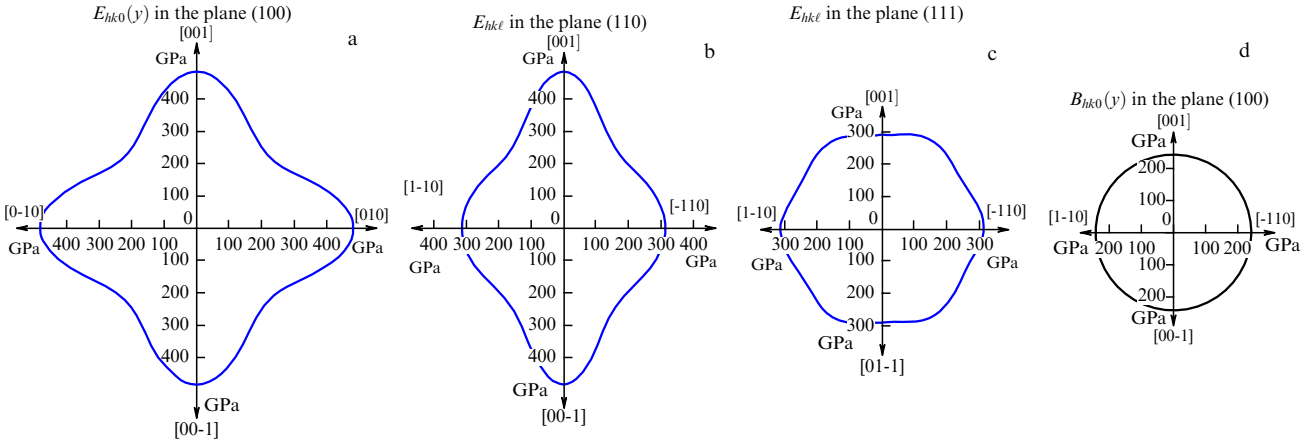

Figure 21. Changes in the Young's modulus E in the crystallographic direction [hkl] in the planes (a) (100), (b) (110), and (c) (111) of cubic Nb_3O_3. The distribution of the bulk modulus B is shown only for the plane (100) (d); the distribution of the modulus B in any other planes has the same form and does not depend on the direction [hkl] [91].

Niobium monoxide does not have a wide homogeneity region and exists in a very narrow range from $NbO_{0.98}$ to $NbO_{1.02}$, close to the stoichiometric composition NbO. This fundamentally distinguishes cubic niobium monoxide from the related cubic monoxides of titanium $TiO_{0.80}$–$TiO_{1.25}$ and vanadium $VO_{0.85}$–$VO_{1.23}$ [1, 84–86], which have very broad homogeneity regions.

The structure of niobium monoxide can be considered in two variants. In the first variant, niobium monoxide Nb_3O_3 has a cubic $B1$-type structure, in which vacancies in the niobium and oxygen sublattices are randomly distributed, and its composition corresponds to $Nb_{0.75}\blacksquare_{0.25}O_{0.75}\square_{0.25}$ (■ and □ are vacant sites in the Nb and O sublattices, respectively). In the second variant, niobium monoxide Nb_3O is considered as an independent phase with a cubic (space group $Pm\bar{3}m$) structure. A characteristic feature of the structure of this phase is that only three of the four sites of each sublattice are occupied by atoms.

According to experimental data [87–89] and calculation results [89, 90], niobium monoxide with a cubic (space group $Pm\bar{3}m$) vacancy-ordered structure Nb_3O_3 does indeed exist and is more energetically favorable compared to Nb_4O_4 with a hypothetical defect-free face-centered cubic structure (space group $Pm\bar{3}m$).

• The elastic constants of cubic Nb_3O_3 monoxide, $c_{11} = 529$, $c_{12} = 101$, and $c_{44} = 112$ GPa, were calculated [91] by the density functional theory method [92] using the generalized gradient approximation. The elastic constants of niobium monoxide Nb_3O_3, presented as a database on the website Materials Projects mp-2331 [93] and equal to $c_{11} = 519$, $c_{12} = 105$, and $c_{44} = 107$ GPa, were calculated *ab initio* using the ELATE code. This code is described in general form in Ref. [94] and is intended for the analysis of elastic stiffness tensors and visualization of anisotropic mechanical properties [77]. The elastic constants of cubic (spatial group $Pm\bar{3}m$) niobium monoxide Nb_3O_3 are significantly lower than in [93] and are equal to $c_{11} = 242$, $c_{12} = 52$, and $c_{44} = 60$ GPa. A comparison of the calculated elastic constants $c_{11} = 529$, $c_{12} = 101$, and $c_{44} = 112$ GPa [91] of cubic (spatial group $Pm\bar{3}m$) niobium monoxide Ni_3O_3 showed that these constants are in good agreement with the data of Ref. [90], whereas the data of Ref. [77] are clearly underestimated. With these facts considered, the calculated elastic stiffness constants $c_{11} = 529$, $c_{12} = 101$, and $c_{44} = 112$ GPa were used to analyze the anisotropy of the Ni_3O_3 monoxide [91].

Figure 21 shows the distributions of Young's modulus E_{hkl} in the (100), (110), and (111) planes for Ni_3O_3 monoxide. The value of Young's modulus E_{hk0} varies from ~ 484 to ~ 313 GPa in the (100) plane, from ~ 484 to ~ 280 GPa in the (110) plane, and from ~ 313 to ~ 280 GPa in the (111) plane. The bulk modulus B does not depend on the direction [hkl]; its distribution is shown only for the (100) plane (Fig. 21d); the value of the modulus B of the monoxide Nb_3O_3 is ~ 243 GPa. The changes in the shear modulus G_{hkl} and the Poisson's ratio μ_{hkl} in the (100), (110), and (111) planes of the Nb_3O_3 monoxide are shown in Fig. 22. The maximum and minimum values of the shear modulus G_{hk0} in the (100) plane are ~ 207 and ~ 122 GPa, and in the (110) and (111) planes they vary from ~ 207 and ~ 107 GPa and from ~ 122 and ~ 107 GPa, respectively (Fig. 22a–c). The Poisson's ratio μ_{hk0} in the (100) plane of niobium monoxide Nb_3O_3 varies from ~ 0.168 to ~ 0.285 depending on the direction [hkl] (see Fig. 11). The value of μ_{hkl} in the (110) plane ranges from ~ 0.168 to ~ 0.308, and in the (111) plane it varies from ~ 0.285 to ~ 0.308 (Fig. 22e, f).

Small changes in the moduli E_{hkl} and G_{hkl} depending on the direction [hkl] indicate weak anisotropy of the elastic properties of cubic Nb_3O_3 monoxide. Indeed, the anisotropy criterion $A_{an} = 2c_{44}/(c_{11} - c_{12})$ [63] for cubic Nb_3O_3 monoxide is equal to ~ 0.52, and the ratio $E_{hkl}^{max}/E_{hkl}^{min}$ is equal to 1.70. This indicates a relatively small anisotropy of the elastic properties of cubic niobium monoxide, close to the anisotropy of stoichiometric cubic niobium and tantalum carbides.

Three-dimensional spatial distributions of Young's modulus E_{hkl} and bulk modulus B_{hkl} of cubic (spatial group $Pm\bar{3}m$) niobium monoxide Nb_3O_3 are shown in Fig. 23. The highest value of Young's modulus E_{max} is observed with external deformation applied along one of the crystallographic directions [001], [010], or [100]. The lowest value E_{min} is observed in eight equivalent directions [$\pm 1 \pm 1 \pm 1$]. The highest and lowest values of Young's modulus of niobium monoxide Nb_3O_3 are ~ 497 and ~ 291 GPa, respectively (see Fig. 23). The bulk modulus B_{hkl} is ~ 243 GPa.

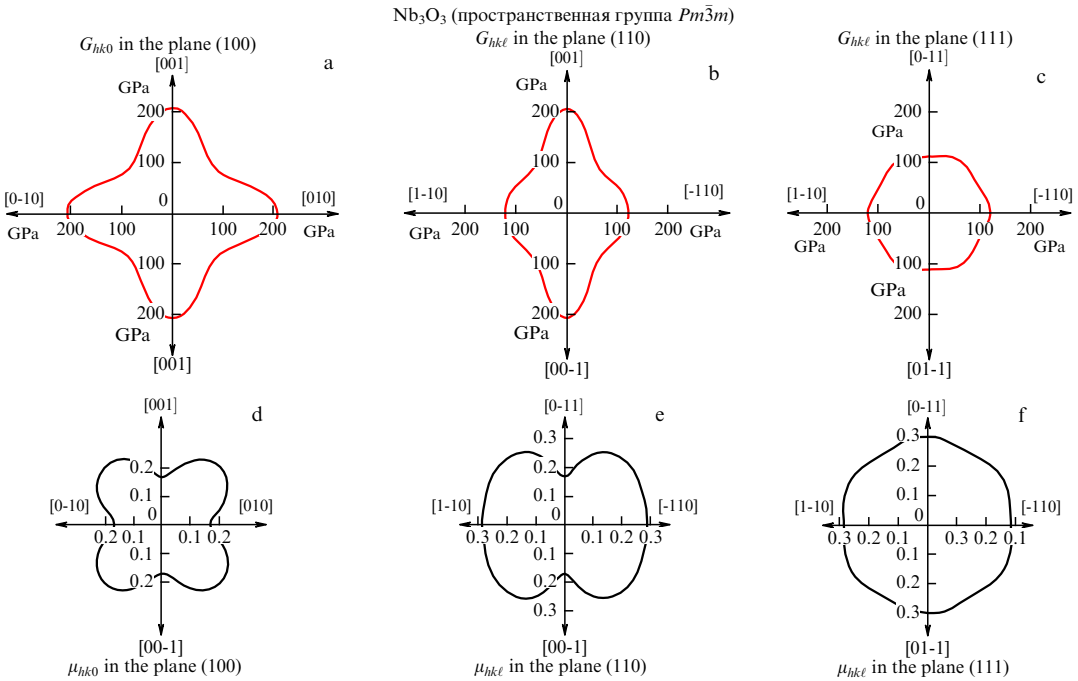

Figure 22. Changes in the shear modulus G_{hkl} and Poisson's ratio μ_{hkl} in the crystallographic direction [hkl] in the (100), (110), and (111) planes of cubic niobium monoxide Nb_3O_3 [91].

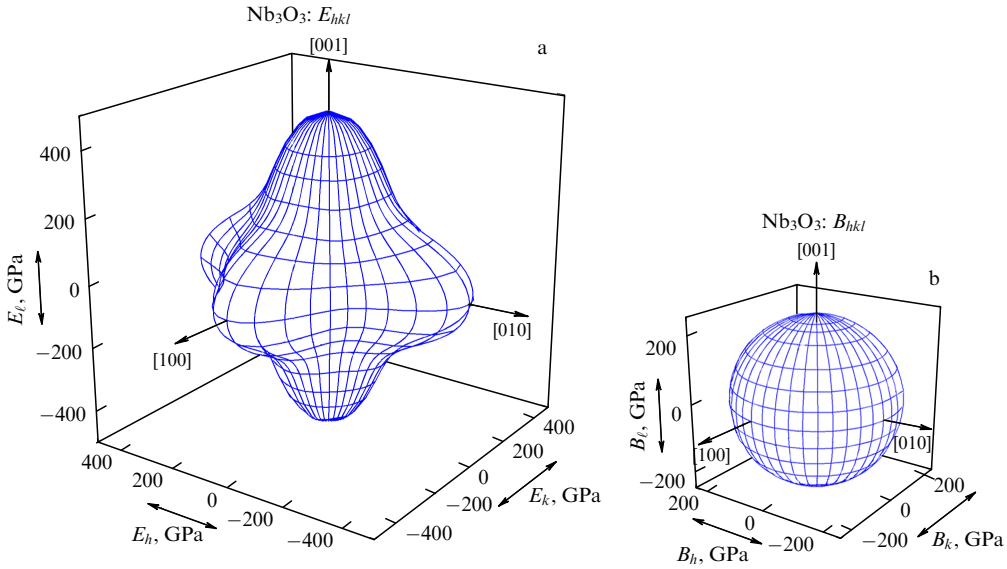

Figure 23. Spatial distributions of (a) Young's modulus E_{hkl} and (b) bulk modulus B_{hkl} of the cubic (spatial group $Pm\bar{3}m$) niobium monoxide Nb_3O_3.

The elastic constants of the described disordered carbides and monoxides are presented in Table 2.

For the monoxides VO_y and Nb_3O_3, data on the elastic properties are extremely limited, but there are no other theoretical studies in the literature on the monoxides VO_y and Nb_3O_3, except for the articles [78] and [92]. Indeed, Ref. [78] is the only theoretical paper on the calculation of the elastic characteristics of the stoichiometric monoxide $VO_{1.00}$ with the $B1$ structure.

Table 3 presents the anisotropy criteria A_{an} and A^U and the ratio $E^{max}_{hkl}/E^{min}_{hkl}$ for cubic titanium monoxides TiO_y, vanadium VO_y, and niobium Nb_3O_3, according to data of Refs [71, 72, 75, 93]. It is evident that titanium monoxide TiO_y has very high anisotropy of elastic properties, whereas the elastic anisotropy of niobium monoxide is significantly lower and close to that of stoichiometric niobium carbide $NbC_{1.0}$ and nonstoichiometric tantalum carbide $TaC_{0.7–0.8}$.

When preparing the manuscript, data from a number of projects of the Materials Project system were used, such as 'mp-910_NbC (Cubic, $Fm\bar{3}m$, 225),' 'mp-1009459_NbC (Cubic, $Pm\bar{3}m$, 221),' 'mp-2664_TiO (Cubic, $Fm\bar{3}m$, 225),' 'mp-1282_VC (Cubic, $Fm\bar{3}m$, 225),' 'mp-21075_HfC (Cubic, $Fm\bar{3}m$, 225),' 'Elastic analysis of TaC (Materials Project id mp-1086),' 'mp-231_1_NbO (Cubic, $Pm\bar{3}m$, 221),' 'mp-2692_NbO (Cubic, $Fm\bar{3}m$, 225)' and other projects for cubic carbides and oxides.

Table 2. Elastic stiffness constants c_{ij} (GPa) and elastic compliance constants s_{ij} (Pa^{-1}) for disordered cubic carbides MC_y and monoxides MO_y with different relative contents y of nonmetallic atoms.

	y	c_{11}	c_{12}	c_{44}	s_{11}	s_{12}	s_{44}
TiC_y	0.50	478.4	106.0	127.4	2.273×10^{-12}	-0.412×10^{-12}	7.852×10^{-12}
	0.55	484.4	107.3	141.2	2.245×10^{-12}	-0.407×10^{-12}	7.081×10^{-12}
	0.60	490.0	108.6	152.6	2.219×10^{-12}	-0.403×10^{-12}	6.555×10^{-12}
	0.65	495.1	109.7	161.4	2.196×10^{-12}	-0.398×10^{-12}	6.197×10^{-12}
	0.70	499.9	110.8	167.7	2.175×10^{-12}	-0.395×10^{-12}	5.964×10^{-12}
	0.75	504.1	111.7	171.4	2.157×10^{-12}	-0.391×10^{-12}	5.834×10^{-12}
	0.80	508.0	112.6	172.6	2.141×10^{-12}	-0.388×10^{-12}	5.792×10^{-12}
	0.85	511.4	113.3	172.3	2.126×10^{-12}	-0.386×10^{-12}	5.802×10^{-12}
	0.90	514.4	114.0	188.4	2.114×10^{-12}	-0.383×10^{-12}	5.307×10^{-12}
	0.95	516.9	114.5	192.0	2.104×10^{-12}	-0.382×10^{-12}	5.209×10^{-12}
	1.00	519.0	115.0	183.0	2.095×10^{-12}	-0.380×10^{-12}	5.465×10^{-12}
ZrC_y	0.60	400.3	90.3	142.9	2.725×10^{-12}	-0.502×10^{-12}	6.996×10^{-12}
	0.65	412.8	93.1	145.1	2.642×10^{-12}	-0.486×10^{-12}	6.889×10^{-12}
	0.70	423.5	95.6	147.1	2.575×10^{-12}	-0.474×10^{-12}	6.796×10^{-12}
	0.75	432.6	97.6	148.9	2.521×10^{-12}	-0.464×10^{-12}	6.717×10^{-12}
	0.80	439.9	99.3	150.4	2.479×10^{-12}	-0.456×10^{-12}	6.649×10^{-12}
	0.85	445.5	100.5	151.7	2.448×10^{-12}	-0.451×10^{-12}	6.594×10^{-12}
	0.90	449.4	101.4	152.7	2.427×10^{-12}	-0.447×10^{-12}	6.550×10^{-12}
	0.95	451.5	101.9	153.5	2.415×10^{-12}	-0.445×10^{-12}	6.517×10^{-12}
	1.00	452.0	102.0	154.0	2.413×10^{-12}	-0.444×10^{-12}	6.494×10^{-12}
HfC_y	0.60	400.3	90.3	142.9	2.725×10^{-12}	-0.502×10^{-12}	6.996×10^{-12}
	0.65	412.8	93.1	145.1	2.642×10^{-12}	-0.486×10^{-12}	6.889×10^{-12}
	0.70	423.5	95.6	147.1	2.575×10^{-12}	-0.474×10^{-12}	6.796×10^{-12}
	0.75	432.6	97.6	148.9	2.521×10^{-12}	-0.464×10^{-12}	6.717×10^{-12}
	0.80	439.9	99.3	150.4	2.479×10^{-12}	-0.456×10^{-12}	6.649×10^{-12}
	0.85	445.5	100.5	151.7	2.448×10^{-12}	-0.451×10^{-12}	6.594×10^{-12}
	0.90	449.4	101.4	152.7	2.427×10^{-12}	-0.447×10^{-12}	6.550×10^{-12}
	0.95	451.5	101.9	153.5	2.415×10^{-12}	-0.445×10^{-12}	6.517×10^{-12}
	1.00	452.0	102.0	154.0	2.413×10^{-12}	-0.444×10^{-12}	6.494×10^{-12}
NbC_y	0.70	351.5	87.9	121.3	3.161×10^{-12}	-0.632×10^{-12}	8.244×10^{-12}
	0.75	429.8	107.5	138.1	2.585×10^{-12}	-0.517×10^{-12}	7.240×10^{-12}
	0.80	493.3	123.3	152.0	2.253×10^{-12}	-0.451×10^{-12}	6.579×10^{-12}
	0.83	524.2	131.0	158.9	2.120×10^{-12}	-0.424×10^{-12}	6.292×10^{-12}
	0.85	541.8	135.4	163.0	2.051×10^{-12}	-0.410×10^{-12}	6.137×10^{-12}
	0.90	575.4	143.9	171.0	1.931×10^{-12}	-0.386×10^{-12}	5.849×10^{-12}
	0.95	594.1	148.5	176.1	1.870×10^{-12}	-0.374×10^{-12}	5.680×10^{-12}
	1.00	598.0	149.5	178.2	1.858×10^{-12}	-0.372×10^{-12}	5.612×10^{-12}
TaC_y	0.70	664.7	127.2	99.3	1.603×10^{-12}	-0.257×10^{-12}	10.068×10^{-12}
	0.75	688.4	131.7	121.8	1.549×10^{-12}	-0.249×10^{-12}	8.212×10^{-12}
	0.80	708.9	135.6	140.3	1.503×10^{-12}	-0.241×10^{-12}	7.128×10^{-12}
	0.85	726.3	139.0	154.9	1.467×10^{-12}	-0.236×10^{-12}	6.457×10^{-12}
	0.90	740.5	141.7	165.5	1.439×10^{-12}	-0.231×10^{-12}	6.042×10^{-12}
	0.95	751.5	143.8	172.2	1.418×10^{-12}	-0.228×10^{-12}	5.806×10^{-12}
	1.00	759.4	145.3	175.0	1.403×10^{-12}	-0.225×10^{-12}	5.714×10^{-12}
TiO_y	0.80	348.2	36.1	19.3	2.929×10^{-12}	-0.275×10^{-12}	51.91×10^{-12}
	0.85	398.5	41.3	22.9	2.559×10^{-12}	-0.240×10^{-12}	43.71×10^{-12}
	0.90	442.4	45.9	26.0	2.305×10^{-12}	-0.217×10^{-12}	38.40×10^{-12}
	0.95	479.9	49.8	28.7	2.125×10^{-12}	-0.200×10^{-12}	34.79×10^{-12}
	1.00	511.0	53.0	31.0	1.996×10^{-12}	-0.188×10^{-12}	32.26×10^{-12}
	1.05	535.7	55.6	32.8	1.904×10^{-12}	-0.179×10^{-12}	30.49×10^{-12}
	1.10	553.9	57.4	34.1	1.841×10^{-12}	-0.173×10^{-12}	29.29×10^{-12}
	1.15	565.7	58.7	35.0	1.803×10^{-12}	-0.169×10^{-12}	28.55×10^{-12}
	1.20	571.1	59.2	35.5	1.786×10^{-12}	-0.168×10^{-12}	28.20×10^{-12}
	1.25	570.1	59.1	35.4	1.789×10^{-12}	-0.168×10^{-12}	28.22×10^{-12}
VO_y	0.75	501.3	138.9	19.5	2.267×10^{-12}	-4.920×10^{-12}	51.16×10^{-12}
	0.80	500.3	138.6	19.4	2.272×10^{-12}	-4.931×10^{-12}	51.43×10^{-12}
	0.85	498.1	138.0	19.3	2.282×10^{-12}	-4.952×10^{-12}	51.90×10^{-12}
	0.90	494.8	137.1	19.0	2.297×10^{-12}	-4.986×10^{-12}	52.57×10^{-12}
	0.95	490.2	135.9	18.7	2.318×10^{-12}	-5.031×10^{-12}	53.46×10^{-12}
	1.00	484.6	134.3	18.3	2.346×10^{-12}	-5.090×10^{-12}	54.60×10^{-12}
	1.05	477.8	132.4	17.9	2.379×10^{-12}	-5.163×10^{-12}	56.02×10^{-12}
	1.10	469.8	130.2	17.3	2.420×10^{-12}	-5.250×10^{-12}	57.74×10^{-12}
	1.15	460.7	127.7	16.7	2.468×10^{-12}	-5.354×10^{-12}	59.83×10^{-12}
	1.20	450.4	124.8	16.0	2.524×10^{-12}	-5.477×10^{-12}	62.36×10^{-12}
	1.25	439.0	121.6	15.3	2.590×10^{-12}	-5.619×10^{-12}	65.41×10^{-12}
Nb_3O_3	0.75	529	101	112	2.413×10^{-12}	-0.348×10^{-12}	9.354×10^{-12}

Table 3. Effect of nonstoichiometry on the elastic stiffness constants c_{ij} (GPa), anisotropy criteria A_{an} and A^U and the ratio $E_{hkl}^{max}/E_{hkl}^{min}$ for cubic titanium monoxides TiO_y, vanadium VO_y and niobium Nd_3O_3 [70, 71, 74, 93].

Monoxide MO_y	y	c_{11}	c_{12}	c_{44}	A_{an}	A^U	E_{hkl}^{max}	E_{hkl}^{min}	$E_{hkl}^{max}/E_{hkl}^{min}$
TiO_y [71, 72]	0.80	348.2	36.1	19.3	0.124	7.468	341.4	55.3	6.18
	1.00	511.0	53.0	31.0	0.135	6.627	501.0	88.6	5.66
	1.20	571.1	59.2	35.5	0.139	6.427	560.0	101.2	5.53
	1.25	576.1	115.0	35.4	0.139	6.417	559.0	101.1	5.53
VO_y [75]	0.80	500.3	138.6	19.4	0.107	8.889	440.2	72.6	6.06
	0.90	494.8	137.1	19.0	0.106	9.909	435.3	71.1	6.10
	1.00	484.6	134.3	18.3	0.105	9.202	426.3	69.2	6.17
	1.10	469.8	130.2	17.3	0.102	9.488	413.3	64.9	6.36
	1.20	450.4	124.8	16.0	0.098	9.899	396.3	60.2	6.58
Nb_3O_3 ($Nb_{0.75}O_{0.75}$) [93]	0.75	529.0	101.0	112.0	0.523	0.521	496.6	291.4	1.70

Figure 24. Distorted octahedron modeling the spatial distribution of the velocity of longitudinal acoustic vibrations from the crystallographic direction for cubic crystals [96].

The three-dimensional spatial distributions of the Young's modulus E_{hkl} of cubic carbides MC_y (M = Ti, Zr, Hf, Nb, Ta) (see Figs 5, 7, 9, 12, 14) and monoxides MO_y (M=Ti, V) (see Figs 17, 20) have the shape of a distorted octahedron (Fig. 24). In the literature, similar dependencies were obtained for the distribution of the velocity of longitudinal acoustic vibrations c_l, (the speed of sound) depending on the crystallographic direction for a single crystal of cubic lead sulfide PbS at 300 K [96]. Later, the authors of Ref. [96], using the data of Ref. [95] and experimental results on the thermal expansion coefficient of a nanocrystalline PbS film, found that the velocities of longitudinal c_l and transverse c_t acoustic vibrations in cubic lead sulfide PbS at $\sim$ 300 K are $\sim$ 3975 and $\sim$ 1881 m s^{-1}. The authors of Ref. [96] constructed spatial distributions of these velocities as functions of the crystallographic direction [hkl] for a PbS single crystal (see Fig. 24). In contrast to the distorted octahedron of longitudinal acoustic vibration velocities, the three-dimensional distributions of elastic moduli of disordered nonstoichiometric cubic carbides and monoxides have smoothed edges and vertices due to the precise consideration of elastic stiffness constants.

5. Melting temperatures of nonstoichiometric carbides TiC_y, ZrC_y, and HfC_y as functions of their elastic constants

Theoretical predictions of melting temperatures and elastic properties have a long history [97]. Such predictions are based on various computational approaches and methods for describing interatomic interactions. In recent decades, density functional theory [92, 98] has established itself as an important tool for general materials modeling. This has been facilitated by the increasing availability of computing power. However, predicting melting temperatures based on DFT remains a challenging task. Theoretical estimates of melting temperatures and elastic properties, typically obtained in various versions of density functional theory, are available only for stoichiometric compounds.

Nonstoichiometric titanium, zirconium, and hafnium carbides (TiC_y, ZrC_y, and HfC_y) with a cubic structure (spatial group $Fm\bar{3}m$) have wide homogeneity regions from $\sim TiC_{0.47–0.50}$ to $TiC_{1.00}$, from $\sim ZrC_{0.60}$ to $ZrC_{1.00}$, and from $\sim HfC_{0.54–0.56}$ to $HfC_{1.00}$, respectively [1, 99]. These carbides are the only compounds in their systems and are among the most refractory compounds, with the highest melting temperature T_m found in nonstoichiometric carbides with a relative carbon content $y < 1.0$. According to the phase diagrams of the Ti–C, Zr–C, and Hf–C systems [99–103], carbides TiC_y, ZrC_y, and HfC_y have melting temperature maxima of $\sim 3340 \pm 20$, $\sim 3710 \pm 20$ and $\sim 4220 \pm 20$ K with a relative carbon content y_m equal to ~ 0.80, ~ 0.82 and ~ 0.94, respectively. Empirical dependences of the melting temperature of various metals and intermetallic compounds, as well as some compounds (silicides, hexaborides, quaternary cubic carbides) on their elastic properties are presented in the literature [104–109]. According to [105], there is a correlation between the elastic modulus and the melting temperature. For example, tungsten, which has the highest melting temperature among cubic metals, has the highest elastic constants among these metals. Empirical relationships between elastic constants and the melting temperature of metals are considered in Ref. [105].

In Ref. [110], an empirical estimate of the melting temperatures T_m of disordered nonstoichiometric cubic carbides TiC_y, ZrC_y, and HfC_y was carried out depending on their composition based on the elastic constants $c_{ij}(y)$ of these carbides. The elastic stiffness constants c_{11}, c_{12}, and c_{44}, found as functions of composition y for these carbides [51, 59, 60], have the form (13)–(15). Carbides TiC_y, ZrC_y, and HfC_y have melting temperature maxima at a relative carbon content y_m equal to 0.80, 0.82 and 0.94, respectively. The

maximum melting temperature of titanium carbide $\sim TiC_{0.80}$ calculated using Eqn (25) is ~ 3344 K, which is 5–6 K higher than the experimental melting temperature of 3338 K according to [104], 5 K higher than the experimental melting temperature of 3339 K according to [105], and approximately 25–26 K higher than the experimental melting temperature of ~ 3308 K of this titanium carbide. The maximum melting temperature of zirconium carbide $\sim ZrC_{0.82}$ calculated using Eqn (25) is ~ 3708 K, and according to experimental data [103] it is 3705 ± 20 K, i.e., the calculation results practically coincide with those of the experiment.

A comparison of experimental data on the melting temperatures T_m of TiC_y, ZrC_y, and HfC_y carbides, performed in Ref. [110], with the elastic rigidity constants $c_{ij}(y)$ found in Refs [51, 59, 60], and their joint analysis allowed us to propose the following empirical dependence of $T_m(y)$ of nonstoichiometric carbides on the values of $c_{11}(y)$ and $c_{44}(y)$:

$$T_m(y) = A\left[3c_{11}(y) + c_{44}(y)\right] - Bc_{11}(y)(y - y_m)^2 + C\,[\mathrm{K}]\,. \quad (25)$$

The presence of the second term proportional to $(y-y_m)^2$ in Eqn (25) ensures the maximum melting temperature of the carbide MC_y in the vicinity of the composition with $y = y_m$; the coefficients A and B are equal to 2 and 20 K/GPa, respectively. The term C is a normalization constant characteristic of a specific carbide; it is equal to -50, $+740$ and $+1030$ K for TiC_y, ZrC_y and HfC_y, respectively. The elastic rigidity constants $c_{11}(y)$ and $c_{44}(y)$ of the carbides MC_y are taken in GPa to estimate the melting temperature. The maximum melting temperature of titanium carbide $\sim TiC_{0.80}$ calculated using Eqn (25) is 3345 K. The maximum melting temperature of zirconium carbide $\sim ZrC_{0.82}$ calculated using Eqn (25) is ~ 3708 K and, according to experimental data [102], practically coincides with $T_m = 3705 \pm 20$ K. According to calculation using relation (25), the maximum melting temperature of $HfC_{0.94-0.95}$ carbide is ~ 4192 K. This is completely consistent with the data of Refs [102, 111], where the maximum melting temperatures T_m are $\sim 4200-4220$ or $\sim 4200 \pm 20$ K, respectively.

Thus, a method is proposed [110] to empirically estimate the melting temperatures T_m of disordered nonstoichiometric cubic carbides TiC_y, ZrC_y, and HfC_y, depending on their composition based on the elastic constants $c_{ij}(y)$ of these carbides. It is established that the carbides TiC_y, ZrC_y, and HfC_y have melting temperature maxima of 3345, 3708, and 4192 K with a relative carbon content y of 0.80, 0.82, and 0.94, respectively. The calculated dependences of the melting temperatures $T_m(y)$ of the carbides TiC_y, ZrC_y, and HfC_y are in qualitative agreement with the phase diagrams of the Ti–C, Zr–C, and Hf–C systems from literature.

Nonstoichiometric titanium, zirconium, and hafnium carbides (TiC_y, ZrC_y, and HfC_y) were chosen because they are the only compounds in their systems, whereas in the Nb–C and Ta–C systems there are still lower carbides M_2C. Empirical relationships between the elastic constants and the melting temperature were previously considered in Ref. [106]. A comparison of the experimental data on the melting temperatures T_m of the TiC_y, ZrC_y, and ZrC_y carbides with the found elastic rigidity constants c_{11}, c_{12} and c_{44} of these carbides and their joint analysis made it possible to propose an empirical dependence of $T_m(y)$ (25) on the values of c_{11} and c_{44}. The second term in Eqn (25), proportional to $(y-y_m)^2$, ensures the maximum melting temperature of a MC_y carbide in the vicinity of the composition with $y = y_m$. Coefficients A and B in Eqn (25) were selected empirically and are equal to 2 and 20 K GPa^{-1}, respectively. The quantity C in Eqn (25) is a normalizing constant characteristic of a particular carbide and was also selected empirically. According to Ref. [106], the elastic constant c_{11} is used to approximate the melting temperature of cubic compounds and intermetallides. The linear combination of elastic constants $(3c_{11} + c_{44})$ in the proposed formula (25) ensures a higher accuracy of melting temperature estimation.

6. Conclusion

This review is the first systematic presentation of the main achievements and results of studies on the elastic characteristics of disordered cubic carbides and oxides TiC_y, ZrC_y, HfC_y, NbC_y, TaC_y, TiO_y, VO_y, and NbO_y, depending on their deviation from stoichiometry. The lack of literature data on the elastic properties of these compounds depending on their composition limited their potential use as functional materials with controlled mechanical properties. A semi-empirical approach to determining elastic constants and estimating elastic anisotropy, developed in Refs [51, 55, 56, 58–60, 70, 71, 91], allowed us to establish for the first time the concentration dependences of the elastic stiffness constants c_{ij} of disordered nonstoichiometric cubic carbides and oxides. The studies showed that all the MX_y compounds considered exhibit anisotropy in their elastic properties, and the elastic stiffness constants $c_{ij}(y)$ are quadratic functions of the composition of these compounds. A comparison of the elastic properties of disordered nonstoichiometric cubic carbides showed that zirconium carbide ZrC_y, whose anisotropy varies slightly with composition y, exhibits the lowest elastic anisotropy throughout the homogeneity region. Low elastic anisotropy is characteristic of titanium carbide TiC_y, but it increases with increasing nonstoichiometry as the lower boundary $TiC_{0.50}$ of the homogeneity region of this carbide is approached. Low elastic anisotropy, which decreases with increasing nonstoichiometry as the lower boundary $NbC_{0.70}$ of the homogeneity region is approached, is observed for niobium carbide NbC_y. Nonstoichiometric tantalum carbide TaC_y is a compound with greater elastic anisotropy than NbC_y carbide. For all the cubic carbides and monoxides considered, the highest Young's and shear moduli are observed in the crystallographic directions $[\pm 100]$, $[0 \pm 10]$, $[00 \pm 1]$, and the lowest Young's and shear moduli are observed in the eight directions $[\pm 1 \pm 1 \pm 1]$. The proposed empirical dependence of the melting temperatures of nonstoichiometric MC_y carbides on their elastic stiffness constants allows us to find the maximum melting temperature as a function of carbide composition. Determining the compositions of MC_y carbides that exhibit reduced brittleness and increased ductility while maintaining high mechanical properties is an important task, the solution of which is possible by changing the nonstoichiometry of the carbides. The established dependences of the elastic properties on the composition of disordered nonstoichiometric cubic compounds TiC_y, ZrC_y, HfC_y, NbC_y, TaC_y, TiO_y, and VO_y open up additional opportunities for targeted control of their properties, ensuring their expanded practical application as materials with high mechanical properties.

In summary, the synthesis, potential engineering applications, and fundamental mechanical properties of disordered

nonstoichiometric cubic carbides and monoxides require further research efforts and a deeper understanding. Due to the possibility of controlling the mechanical and elastic properties of disordered nonstoichiometric cubic carbides and monoxides by varying their composition, such compounds are excellent candidates for widespread application. It can be expected that more and more researchers will study these unique materials and make significant scientific advances in the field of the influence of nonstoichiometry on the elastic properties of solids.

This work was carried out under the State Assignment of the Ministry of Education and Science of the Russian Federation FUWF-2024-0010 No. 124020600013-9. Research on niobium carbide and oxide was conducted with financial support from the Russian Science Foundation (Project No. 19-73-20012-P, https://rscf.ru/en/project/19-73-20012/) at the Institute of Solid State Chemistry, Ural Branch of the Russian Academy of Sciences.

References

1. Gusev A I, Rempel A A, Magerl A J *Disorder and Order in Strongly Nonstoichiometric Compounds. Transition Metal Carbides, Nitrides and Oxides* (Springer Series in Materials Science, Vol. 47) (Berlin : Springer, 2001) DOI:10.1007/978-3-662-04582-4
2. Gusev A I *Nestekhiometriya, Besporyadok, Blizhnii i Dal'nii Poryadok v Tverdom Tele* (Nonstoichiometry, Disorder, Short-Range and Long-Range Order in Solids) (Moscow: Fizmatlit, 2007)
3. Storms E K (Ed.) *Refractory Materials* Vol. 2 *The Refractory Carbides* (New York: Academic Press, 1967)
4. Holleck H *Binäre und Ternäre Carbid- und Nitridsysteme der Übergangsmetalle* (Materialkundlich-Technische Reihe, Nr. 6, Hrsg. G Petzow) (Berlin: Gebrüder Borntraeger, 1984)
5. Shabalin I L *Ultra-High Temperature Materials II. Refractory Carbides I* (Ta, Hf, Nb *and* Zr *Carbides*) (Dordrecht: Springer, 2019) DOI:10.1007/978-94-024-1302-1
6. Bauccio M (Ed.) *ASM Engineering Materials Reference Book* 2nd ed. (Materials Park, OH: ASM Intern., 1994)
7. Upadhyaya G S *Nature and Properties of Refractory Carbides* (Commack, NY: Nova Science Publ., 1996)
8. Gogotsi Y G, Andrievski R A (Eds) *Materials Science of Carbides, Nitrides and Borides* (NATO Science Partnership Subser. 3, Vol. 68) (Dordrecht: Kluwer Acad. Publ., 1999) DOI:10.1007/978-94-011-4562-6
9. Ramqvist L *Jernkontorets Annaler* **152** 467 (1968)
10. Ramqvist L *Jernkontorets Annaler* **152** 517 (1968)
11. Kral C et al. *J. Alloys Compd.* **265** 215 (1998)
12. Valeeva A A et al. *Russ. Chem. Rev.* **90** 601 (2021); *Usp. khim.* **90** 601 (2021)
13. Yang Y et al. *J. Alloys Compd.* **485** 542 (2009)
14. Krasnenko V, Brik M G *Solid State Sci.* **14** 1431 (2012)
15. Luo Y-T, Chen Z-Q, in *Intern. Symp. on Materials Application and Engineering, SMAE 2016, 20–21 August 2016, Chiang Mai, Thailand* (MATEC Web Conf. Volume 67, Eds M Jawaid et al.) (Les Ulis Cedex A: EDP Sciences, 2016) p. 06014, DOI:10.1051/matecconf/20166706014
16. Zhang J, McMahon J M *J. Mater. Sci.* **56** 4266 (2021)
17. Ahmed R et al. *J. Mater. Res. Technol.* **24** 4808 (2023)
18. Landau L D, Lifshitz E M *Theory of Elasticity* (Oxford: Pergamon Press, 1959)
19. Fedorov F I *Theory of Elastic Waves in Crystals* (New York: Plenum Press, 1968) DOI:10.1007/978-1-4757-1275-9
20. Nye J F *Physical Properties of Crystals. Their Representation by Tensors and Matrices* (Oxford: Clarendon Press, Oxford Univ. Press, 1985)
21. Weber W *Phys. Rev. B* **8** 5082 (1973)
22. Ahuja R et al. *Phys. Rev. B* **53** 3072 (1996)
23. Amriou T et al. *Physica B* **25** 46 (2003)
24. Cheng D, Wang S, Ye H *J. Alloys Compd.* **377** 221 (2004)
25. Wu Z et al. *Phys. Rev. B* **71** 214103 (2005)
26. López-de-la-Torre L et al. *Solid State Commun.* **134** 245 (2005)
27. Zaoui A, Bouhafs B, Ruterana P *Mater. Chem. Phys.* **91** 108 (2005)
28. He L F et al. *Scripta Mater.* **58** 679 (2008)
29. Ivashchenko V I, Turchi P E A, Shevchenko V I *J. Phys. Condens. Matter* **21** 395503 (2009)
30. Li Y et al. *Sci. China Phys. Mech. Astron.* **54** 2196 (2011)
31. Wang X et al. *Trans. Nonferrous Met. Soc. China* **21** 1373 (2011)
32. Feng W et al. *Physica B* **406** 3631 (2011)
33. Aksyonov D A, Lipnitskii A G, Kolobov Yu R *Comput. Mater. Sci.* **65** 434 (2012)
34. Srivastava A, Diwan B D *Can. J. Phys.* **90** 331 (2012)
35. Zeng Q et al. *Phys. Rev. B* **88** 214107 (2013)
36. Wu L et al. *J. Alloys Compd.* **561** 220 (2013)
37. Liu Y et al. *J. Alloys Compd.* **582** 500 (2014)
38. Ma S-Q et al. *Commun. Theor. Phys.* **62** 895 (2014)
39. Dang D Y, Fan J L, Gong H R *J. Appl. Phys.* **116** 033509 (2014)
40. Yu X-X, Weinberger C R, Thompson G B *Acta Mater.* **80** 341 (2014)
41. Xie C et al. *Phys. Chem. Chem. Phys.* **18** 12299 (2016)
42. Jiang M et al. *Sci. Rep.* **7** 9344 (2017)
43. Glechner T et al. *Sci. Rep.* **8** 17669 (2018)
44. Hong D et al. *Physica B* **558** 100 (2019)
45. Jubair M et al. *J. Phys. Commun.* **3** 055017 (2019)
46. Sun W et al. *Phys. Chem. Chem. Phys.* **22** 5018 (2020)
47. Oganov A R, Glass C W *J. Chem. Phys.* **124** 244704 (2006)
48. Kresse G, Furthmüller J *Comput. Mater. Sci.* **6** 15 (1996)
49. Kresse G, Furthmüller J *Phys. Rev. B* **54** 11169 (1996)
50. Kresse G, Joubert D *Phys. Rev. B* **59** 1758 (1999)
51. Gusev A I *Phys. Chem. Chem. Phys.* **23** 18558 (2021)
52. Wolf W et al. *Philos. Mag. B* **79** 839 (1999)
53. Sadovnikov S I *JETP Lett.* **112** 193 (2020) DOI:10.1134/S0021364020150096; *Pis'ma Zh. Eksp. Teor. Fiz.* **112** 203 (2020) DOI:10.31857/ S1234567820150100
54. Sadovnikov S I, Gusev A I *Phys. Chem. Chem. Phys.* **23** 2914 (2021)
55. Valeeva A A, Gusev A I *Int. J. Refract. Met. Hard Mater.* **95** 105435 (2021)
56. Gusev A I *Phys. Solid State* **64** 2173 (2022) DOI:10.21883/PSS.2022.13.52322.151; *Fiz. Tverd. Tela* **63** 1921 (2021) DOI:10.21883/ FTT.2021.11.51598.151
57. Kostenko M G, Gusev A I, Lukoyanov A V *Acta Mater.* **223** 117449 (2022)
58. Gusev A I *Int. J. Refract. Met. Hard Mater.* **103** 105760 (2022)
59. Gusev A I *Int. J. Refract. Met. Hard Mater.* **113** 106192 (2023)
60. Gusev A I *Int. J. Refract. Met. Hard Mater.* **120** 106602 (2024)
61. Newnham R E *Properties of Materials. Anisotropy, Symmetry, Structure* (New York: Oxford Univ. Press, 2005)
62. Gnäupel-Herold T, Brand P C, Prask H J *J. Appl. Cryst.* **31** 929 (1998)
63. Gnäupel-Herold T, Brand P, Prask H J, in *Advances in X-ray Analysis, Proc. of the 47th Denver X-Ray Conf., August 3–7, 1998, Colorado Springs* (Adv. in X-ray Analysis, Vol. L42) (Newtown Square, PA: ICDD, 1998) p. 464; https://www.icdd.com/assets/resources/axasearch/VOL42/V42_54.pdf
64. Atkins A G, Tabor D *Proc. R. Soc. London A* **292** 441 (1966) DOI:10.1098/rspa.1966.0146
65. Samsonov G V et al. *Phys. Status Solidi A* **1** 327 (1970)
66. Zhang J-M et al. *J. Phys. Chem. Solids* **68** 503 (2007)
67. Zener C *Elasticity and Anelasticity of Metals* (Chicago, IL: Univ. of Chicago Press, 1948)
68. Ranganathan S I, Ostoja-Starzewski M *Phys. Rev. Lett.* **101** 055504 (2008)
69. Hill R *Proc. Phys. Soc. A* **65** 349 (1952)
70. Valeeva A A, Gusev A I *Phys. Solid State* **66** 761 (2024); *Fiz. Tverd. Tela* **85** 789 (2024)
71. Gusev A I, Valeeva A A *Mendeleev Commun.* **34** 647 (2024) DOI:10.1016/j.mencom.2024.09.007
72. Valeeva A A et al. *Inorg. Mater.* **53** 1174 (2017); *Neorg. Mater.* **53** 1194 (2017)
73. Pugh S F *Philos. Mag.* **45** 823 (1954)
74. Gusev A I *JETP Lett.* **121** 864 (2025); *Pis'ma Zh. Eksp. Teor. Fiz.* **121** 903 (2025)
75. Geld P V, Alyamovskii S I, Matveenko I I *Zh. Strukt. Khim.* **2** 301 (1961)
76. Valeeva et al. *Inorg. Mater.* **45** 905 (2009); *Neorg. Mater.* **45** 975 (2009)

77. Cinthia A J et al. *Int. J. Sci. Eng. Res.* **5** 1 (2014)
78. Teter D M *MRS Bull.* **23** 22 (1998)
79. Chen X-Q et al. *Intermetallics* **19** 1275 (2011)
80. Andersson G, Magneli A *Acta Chem. Scand.* **11** 1065 (1957) DOI:10.3891/acta.chem.scand.11-1065
81. Bowman A L et al. *Acta Cryst.* **21** 843 (1966)
82. Burdett J K, Hughbanks T *J. Am. Chem. Soc.* **106** 3101 (1984)
83. Ha N N *Opt. Spectrosc.* **115** 233 (2013) DOI:10.1134/S0030400X13080134; *Opt. Spektrosk.* **115** 272 (2013) DOL10.7868/ S003040341308014X
84. Andersson S et al. *Acta Chem. Scand.* **11** 1641 (1957) DOI:10.3891/acta.chem.scand.11-1641
85. Banus M D, Reed T B, Strauss A J *Phys. Rev. B* **5** 2775 (1972)
86. Gusev A I, Davydov D A, Valeeva A A *J. Alloys Compd.* **509** 1364 (2011)
87. Hulm J K et al. *J. Low. Temp. Phys.* **7** 291 (1972)
88. Okaz A M, Keesom P H *Phys. Rev. B* **12** 4917 (1975)
89. Efimenko A K et al. *Phys. Rev. B* **96** 195112 (2017)
90. Schulz W W, Wentzcovitch R M *Phys. Rev. B* **48** 16986 (1993)
91. Gusev A I *Solid State Commun.* **372** 115310 (2023)
92. Kohn W, Sham L J *Phys. Rev.* **140** A1133 (1965)
93. NbO, mp-2311. Materials Explorer. The Materials Project, https://materialsproject.org/materials/mp-2311
94. Gaillac R, Pullumbi P, Couder F-X *J. Phys. Condens. Matter* **28** 275201 (2016)
95. Chudinov A A *Sov. Phys. Solid State* **5** 1061 (1963); *Fiz. Tverd. Tela* **5** 1459 (1963)
96. Sadovnikov S I, Gusev A I *J. Alloys Compd.* **610** 196 (2014)
97. Frenkel D, Smit B *Understanding Molecular Simulation*: *From Algorithms to Applications* 2nd ed. (San Diego, CA: Academic Press, 2002) DOI:10.1016/B978-0-12-267351-1.X5000-7
98. Hohenberg P, Kohn W *Phys. Rev.* **136** B864 (1964)
99. Rudy E, Harmon D P, Brukl C E, in *Ternary Phase Equilibria in Transition Metal–Boron–Carbon–Silicon Systems* (AFML-TR-65-2, Pt. 1, Vol. 2, Eds E Rudy, D P Harmon) (Dayton, OH: Wright-Patterson Air Force Base, 1965) p. 1
100. Okamoto H *J. Phase Equilibria Diffusion* **27** 306 (2006)
101. Okamoto H *J. Phase Equilibria* **17** 162 (1996)
102. Okamoto H *Bull. Alloy Phase Diagrams* **11** 396 (1990)
103. Sara R V *J. Am. Ceram. Soc.* **48** 243 (1965)
104. Seifert H J, Lukas H L, Petzow G *J. Phase Equilibria* **17** 24 (1996)
105. Fine M E, Brown L D, Marcus H L *Scripta Metallurg.* **18** 951 (1984)
106. Alouani M, Albers R C, Methfessel M *Phys. Rev. B* **43** 6500 (1991)
107. Wang S-L, Pan Y *J. Am. Ceram. Soc.* **102** 4822 (2019)
108. Pan Y, Chen S, Jia Y *RSC Adv.* **9** 33625 (2019)
109. Liu S-Y et al. *J. Eur. Ceram. Soc.* **41** 6267 (2021)
110. Gusev A I *Int. J. Refract. Met. Hard Mater.* **126** 106920 (2025)
111. Rudy E, in *Ternary Phase Equilibria in Transition Metal–Boron–Carbon–Silicon Systems* (AFML-TR-65-2. Pt. 1. Related Binary Systems, Vol. 4 , Eds E Rudy, D P Harmon) (Dayton, OH: Wright-Patterson Air Force Base, 1965) p. 1